FFG-Programm/Instrument: ASAP 9

ENDBERICHT

FFG Projektnummer	840089	**eCall Antragsnummer**	3589434
Kurztitel	MAQROsteps	**FörderungsnehmerIn**	FFG
Bericht Nr.	840089-2	**Berichtszeitraum**	08/2013 – 07/2015
Bericht erstellt von	Rainer Kaltenbaek		

Richtwert für den Umfang: 30-40 Seiten

1. Zusammenfassung Deutsch/Englisch (je eine Seite)

Geben Sie eine Zusammenfassung der im gesamten Berichtszeitraum erfolgten Arbeiten. Beim Endbericht sollen alle Berichtszeiträume zusammengefasst werden.

Ziele und Ergebnisse

- Wurden die dem Förderungsvertrag zugrunde liegenden Ziele erreicht? Sind diese Ziele noch aktuell bzw. realistisch? (Achtung: Änderungen von Zielen erfordern eine Genehmigung durch die FFG)
- Vergleichen Sie die Ziele mit den erreichten Ergebnissen.
- Beschreiben Sie „Highlights" und aufgetretene Probleme bei der Zielerreichung.

GERMAN:

Die Systemanalyse und Projektplanung (WP 1.1 & WP 1.2) wurden wie geplant durchgeführt und abgeschlossen.

Die Thermalstudie des Hitzeschildes für MAQRO (WP 2.1) wurde schon früher als geplant erfolgreich abgeschlossen. Insbesondere hat WP 2.1 sogar Resultate produziert, die signifikant über die erwarteten Resultate hinausgehen: wir haben in einem zweiten Arbeitsschritt nicht nur eine weit detailliertere Thermalanalyse durchgeführt, sondern wir haben auch ausgiebige Studien dazu gemacht, wie sich der Thermalschild bei verschiedenen Optimierungen der Struktur verhält sowie in zwei missionsrelevanten Orbitszenarien. Auf den Temperaturen beruhend, die von unserem Thermalmodel für die die optische Bank und das „Testvolumen" vorhergesagt werden, haben wir unsere früheren Abschätzungen für das erreichbare Vakuum neu evaluiert (WP 2.2). Wir folgern, dass die Schildstruktur es erlauben wird, die technischen Anforderungen der MAQRO Mission zu erfüllen. Wir haben ein Paper zu den detaillierteren Resultaten (WP 2.1) zur Veröffentlichung bei Applied Thermal Engineering eingereicht, wo es zurzeit unter Begutachtung ist. Die Thermalstudie im ursprünglich geplanten Ausmaß wurde bereits 2014 veröffentlicht.

Während dieses ersten Berichtzeitraumes haben wir ein neuartiges Design für eine Kombination von Feed-Back Kühlen und Seitenbandkühlen entwickelt (WP 3.1), welches die Grundlage für unsere experimentelle Arbeit in WP 3.2 und WP 3.3 bildete. In diesen Arbeitspaketen haben wir große Fortschritte erzielt, die voraussichtlich innerhalb der nächsten Monate reif zur Veröffentlichung sein werden. Zudem ist einer Veröffentlichung der theoretischen Grundlagen unserer neuen Methode des 3D Kühlens in Vorbereitung, wie noch im Zusammenhang der Arbeitspakete WP 3.1, WP 3.2, WP 3.3 und WP 4.3 weiter unten beschrieben wird.

Wir haben erfolgreich ein Design für zwei adhesively bonded Cavities erstellt (WP4.1). Beide Designs wurden implementiert (WP4.2). Eine der beiden Cavities wurde mittlerweile vollständig charakterisiert, und die zweite Cavity wurde implementiert und wird kurz nach Projektende vollständig charakterisiert werden. Zu den Arbeiten am ersten Design ist das Manuskript für eine Veröffentlichung praktisch fertig und wird nur noch kleine Überarbeitungsschritte brauchen, bevor es zur Veröffentlichung eingereicht wird.

Des Weiteren haben wir eine vollständig neue Vakuumkammer designed mit dem Ziel, eine unserer adhesively bonded Cavities auf zu nehmen. Diese Vakuumkammer wurde in zwei Ausführungen gebaut – eine für Vorabtests, und eine weitere für das tatsächliche Setup für optomechanische Experimente. Zusätzlich erlaubt die neue Vakuumkammer die Integration mit neuen Mechanismen zum Laden von Testteilchen in die optische Falle. Unser optomechanisches Setup vereint dadurch auf einzigartige Weise neue Methoden des Teilchenladens und des Teilchentransports, eine hochstabile optomechanische Cavity und eine neue Methode des optomechanischen Kühlens. MAQROsteps hat dadurch massiv zu entscheidenden Fortschritten zu weltführenden Experimenten zur Quantenoptomechanik mit optisch gefangenen Teilchen beigetragen – ein entscheidender Schritt in der Technologieentwicklung in Bezug auf das Missionsproposal MAQRO.

ENGLISH:

System engineering and study management (WP 1.1 & WP 1.2) have proceeded and were concluded as planned, and there are no deviations to be reported.

The thermal study of the heat shield for MAQRO (WP 2.1) was successfully concluded already earlier than scheduled. In particular, WP 2.1 produced results going even significantly beyond what we originally expected: in a second work step, we did not only perform a more detailed thermal analysis, but we also performed detailed studies on how the thermal shield would behave under various optimizations of the shield structure and in two mission relevant orbital cases. Based on the temperatures predicted for the optical bench of the instrument and of the “test volume”, we re-evaluated our earlier estimates for the vacuum achievable (WP 2.2). We concluded that the shield structure will allow meeting the technical requirements of the MAQRO mission proposal. We have submitted a paper on the more detailed results (WP 2.1) for publication in Applied Thermal

Engineering, where it is currently under review. The thermal study in its originally intended extent was already published in 2014.

In the course of this project, we have devised a novel design for combining feedback and side-band cooling (WP 3.1), which formed the basis for our experimental work in WP 3.2 and WP 3.3. In these work packages, we have achieved significant progress that should lead to publishable results within the next few months. Moreover, we are working on a publication of the theoretical principles behind our novel method for 3D optomechanical cooling, which will be described below in the context of the work packages WP 3.1, WP 3.2, WP 3.3 and WP 4.3.

We successfully worked out designs for two adhesively bonded cavities (WP 4.1). Both designs were implemented (WP 4.2). One of the cavities has by now been fully characterized, and the second cavity was implemented and will be fully characterized shortly after the end of this project. With respect to our work on the first design, we are essentially finished with a manuscript for publication. It will only take a little more review before submission.

Moreover, we designed a completely new vacuum chamber with the goal that it will hold one of our adhesively bonded cavities. We implemented two of these new vacuum chambers – one for preliminary testing, the other is in use in the actual optomechanical experimental setup. In addition, the new vacuum chamber allows the integration of novel mechanisms for loading test particles into the optical trap. In this way, our optomechanical setup uniquely combines new methods of particle loading and transport, a highly stable optomechanical cavity and a novel method of optomechanical cooling. MAQROsteps has contributed massively to substantial progress towards state-of-the-art experiments on quantum optomechanics with optically trapped particles – an important step of technology development for the MAQRO mission proposal.

2. Arbeitspakete und Meilensteine

2.1 Übersichtstabellen

Tabelle 1: Arbeitspakete

AP Nr.	Arbeitspaket Bezeichnung	Fertigstellungsgrad	Basistermin		Aktuell		Erreichte Ergebnisse / Abweichungen
			Anf.	Ende	Anf.	Ende	
1.1	Prime contractor system engineering and study management	100%	04/2013	03/2015	08/2013	07/2015	The project management is operating within expectations.
1.2	Local system engineering and study management	100%	04/2013	03/2015	08/2013	07/2015	The project management is operating within expectations. Because the work packages of the sub-contractor have been finished, only the dissemination of the results is still pending.

2.1	Thermal design study	100%	04/2013	03/2014	08/2013	06/2014	The thermal design study exceeded expectations in its details and results. One part published, the second paper is currently in review.
2.2	Vacuum analysis	100%	04/2014	05/2014	04/2014	06/2014	Successfully concluded.
3.1	Design for cooling schemes	100%	04/2013	05/2013	08/2013	09/2013	Theoretical methods behind our novel 3D cooling scheme nearly ready for publication.
3.2	Implementation of feed-back cooling	80%	06/2013	11/2013	10/2013	06/2015	First promising results have been achieved, setup is being optimized.
3.3	Implementation of side-band cooling	80%	12/2013	08/2014	04/2014	06/2015	First promising results have been achieved, setup is being optimized.
4.1	Design of bonded cavity	100%	09/2014	09/2014	10/2013	11/2013	Successfully concluded.
4.2	Implementation of bonded cavity	100%	10/2014	11/2014	01/2014	07/2015	Implemented two cavity designs, fully characterized the one to be integrated with the optomechanical setup, MAQRO demonstration cavity still to be characterized. Publications in progress.
4.3	Feed-back & side-band cooling with bonded cavity	80%	12/2014	03/2015	04/2015	07/2015	Novel vacuum chambers designed and implemented, cavity holder for bonded cavity flawed. Can be integrated with optomechanical setup as soon as cavity holder can be replaced with correct design. Not finished within project duration but only positive deviations from existing setup expected. Will be realized very soon.

Tabelle 2: Meilensteine

Meilen-stein Nr.	Meilenstein Bezeichnung	Basis-termin	Akt. Planung	Meilenstein erreicht am	Anmerkungen zu Abweichungen
1	Critical design review for cooling schemes	06/2013	10/2013	22.10.2013	Successfully held within schedule.
2	Review of space-related analyses	06/2014	01/2014	24.01.2014	Successfully held within schedule.
3	Post-test review for feed-back cooling	12/2013	05/2015	04.05.2015	Successfully completed.
4	Post-test review for side-band cooling	09/2014	05/2015	04.05.2015	Successfully completed.
5	Critical design review for bonded cavity	10/2014	05/2015	04.05.2015	Successfully completed.
6	Test-readiness review for bonded cavity	12/2014	07/2015	01.07.2015	Successfully completed.
7	Final review	04/2015	08/2015	25.08.2015	Successfully completed.

2.2 Beschreibung der im Berichtszeitraum durchgeführten Arbeiten

The local as well as the overall system engineering and study management (**WP1.1** and **WP 1.2**) operated and were concluded within schedule.

Work packages WP 2.1 and WP 2.2

The thermal design study **(WP 2.1)** was a full success: it demonstrated that our shield design should be able to allow fulfilling the thermal requirements of MAQRO, and our thermal study could be concluded already ahead of schedule. A paper on the first results was already published in 2014 (Ref.[1]). This paper was also featured in BBC Future[2]. Figure 1 shows the corresponding shield design and defines the geometrical parameters we optimized in the course of the study.

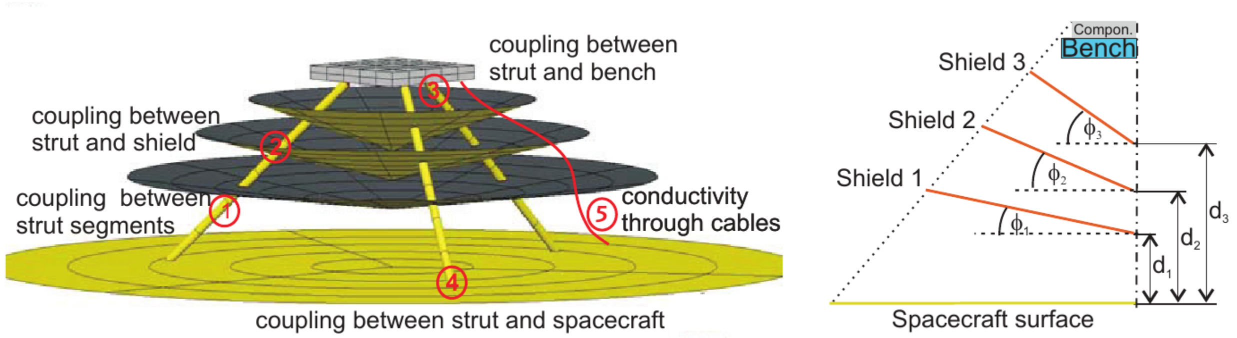

Figure 1: (left) Geometrical model of the shield structure, and how the shields are connected to the spacecraft. (right) Parameters defining the geometrical shield structure – relative distances and angles.

An important detail we noticed in our study is that the immediate volume around the position where our nanoparticle will be trapped – the **"test volume"** – can be significantly colder than the optical bench itself. In particular, if the optical bench below the test volume is coated with gold, thermal radiation will mainly be radiated from other (not cold-coated) parts of the optical bench (OB). The effect of gold coating on the temperature of the test volume is illustrated in Figure 2 (d). Panel (a) of that figure shows the optimization of the opening angle of the shields and their distance to the spacecraft. Panel (b) shows the dependence of the OB temperature on the thermal coupling between strut segments and between struts and shields. Panel (c) shows the dependence of the OB temperature on the dissipation of the "CCD head". **Important note:** in the past, we sometimes referred to the detector chip on the OB as a CCD head. To be correct, this is actually a CMOS chip. In our design, this detector chip is connected to a CMOS pre-processing chip located behind the first thermal shield. This design is based on technological heritage from the MIRI instrument of the James Webb Space Telescope (JWST), and a realistic design goal seems to be for the dissipation of the CMOS detector chip to be about 1mW while the dissipation of the preprocessing chip may be around 10mW[3].

The thermal study itself was performed using a finite-element model and the ESATAN-TMS software[4]. It included radiative as well as conductive thermal coupling. We chose the temperature of the spacecraft (300 K) and the temperature of deep space (~3 K) as boundary conditions for our thermal model. Figure 3 shows the resulting temperature distribution on the optical bench. For the test volume, the thermal model predicted a temperature of 16.4 K – significantly colder than the average temperature of the optical bench (~ 27 K).

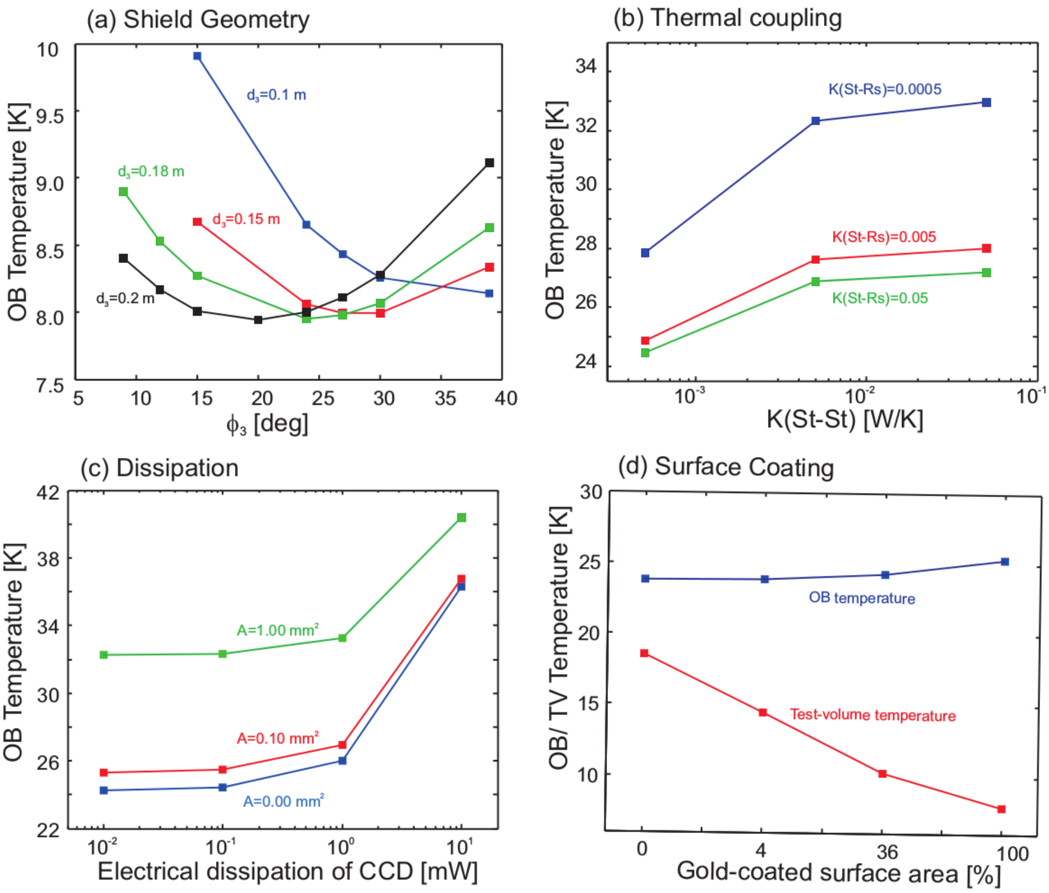

Figure 2: (a) Optimization of the shield opening angle for different distances of the shields to the spacecraft. **(b)** Temperature of the optical bench (OB) for various thermal couplings between struts and radiation shields (St-Rs) as a function of the thermal coupling between strut elements. **(c)** OB temperature as a function of the power dissipated by the bench CCD chip – for various values of the cross-section area of the electrical harness (A). **(d)** Temperatures of the OB and the test volume as a function of the percentage of the gold-coated surface area.

Our model included anticipated electrical and optical dissipation on the optical bench. The model showed that the collimating lens of the on-bench imaging system limited the minimum temperature achievable for the test volume. When removing this lens, the test volume cooled down to ~12 K.

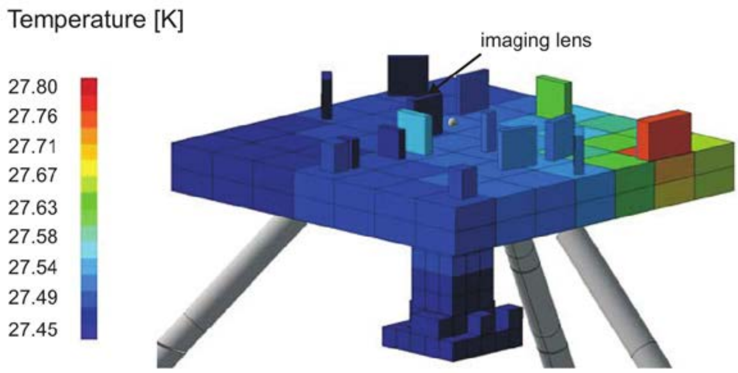

Figure 3: Temperature distribution on the optical bench. The hottest part is the CCD head. The gray sphere indicates the test volume.

In late 2013, we began a more detailed thermal study, and we concluded it in spring 2014. In particular, we did not only improve the design of the optical bench of MAQRO in order to achieve lower temperatures, but we also investigated different orbital scenarios as well as modifications of the size of the heat shield, material of the optical bench, the multi-layer insulation (MLI) of the shields and the optimal amount of gold-coating for the optical bench. A paper on these results has been published on arXiv [5] and is currently under consideration for *Applied Thermal Engineering*.

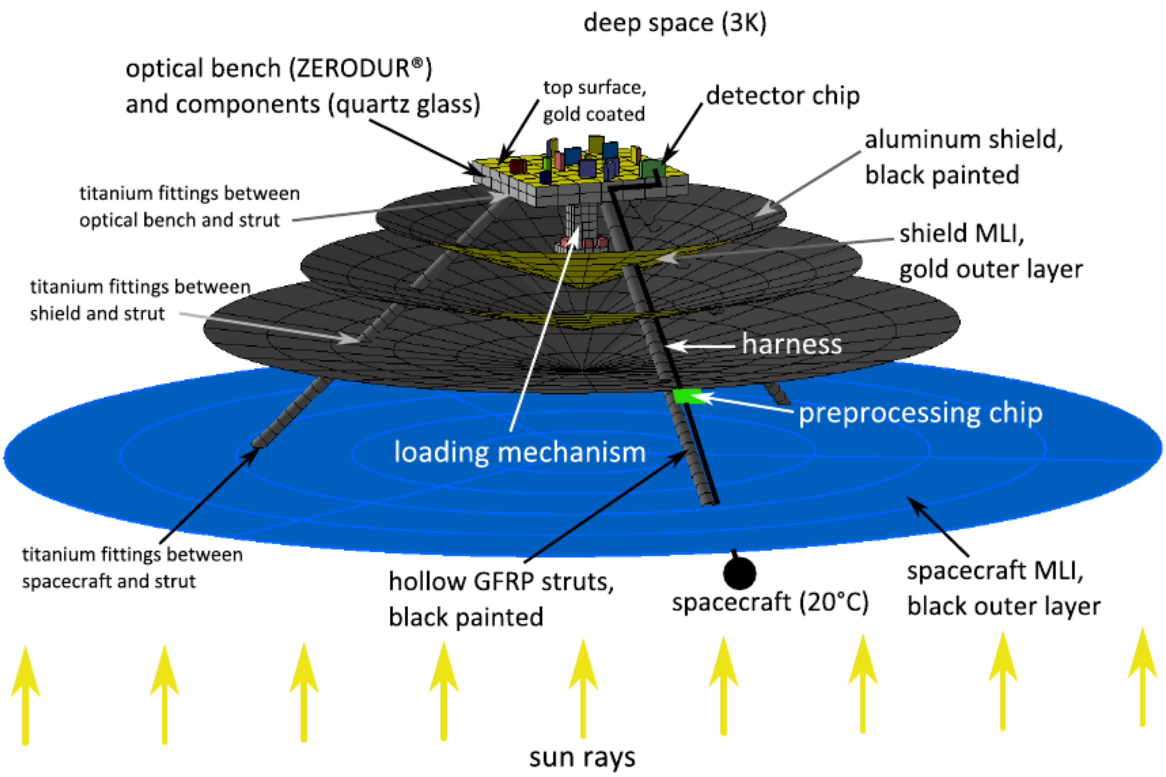

Figure 4: Geometrical model from the more detailed thermal study. The black line indicates the electrical harness. The optical fibres are not drawn because their influence on the temperature proved to be negligible. The CCD preprocessing chip is assumed to be located beneath the first shield.

Figure 4 shows the geometrical model we used for this more detailed study. The sun rays are mostly or completely shielded from the thermal shield structure by the spacecraft, depending on the radius of the shields.

As discussed earlier, an imaging lens limited the temperature achievable for the test volume in the first thermal study. For the second thermal study, we modified the optical-bench setup as illustrated in Figure 5. This design also took into account our bonded-cavity design for the present project MAQROsteps, which will be described in more detail below. Moreover, for the new thermal study, we moved the test volume closer to the second cavity mirror and away from the particle feed-through (FT) in the optical bench because through this hole, the test volume would have the hot loading mechanism in its field of view.

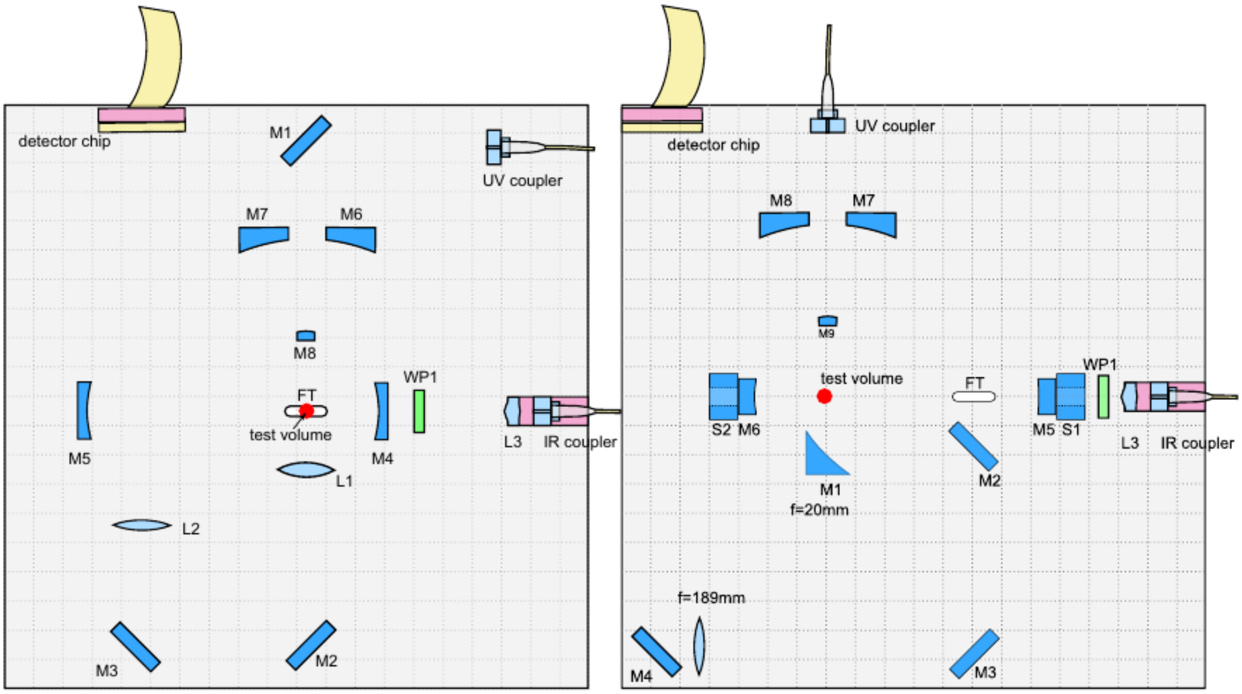

Figure 5: Because our first thermal study showed that the imaging lens L1 in the original bench design (left) limited the temperature achievable for the test volume, we designed a novel setup (right) where the lens was replaced by a parabolic mirror (M1), and we moved the test volume away from the feed-through (FT) hole in the optical bench where particles are fed through from the loading mechanism. The "spacers" S1 and S2 on which the cavity mirrors are mounted reflect the bonded-cavity design we implement in MAQROsteps.

gold area [cm^2]	temperature [K]		radiated heat [µW]	
	test volume	optical bench	$\varepsilon = 0.02$ gold area	$\varepsilon = 0.80$ area
0	18.4	23.1	-	447
73.5	12.4	23.3	2.17	385
204	11.1	23.7	6.70	242
400	11.1	24.4	14.1	-

Table 1: For the new optical bench design, we again investigated the influence of coating part of the OB surface with f

For the new thermal study, we again analyzed the influence of gold-coating of the optical bench on the temperature of the test volume. Table 1 shows results of this analysis – the larger the gold-coated area, the lower the temperature of the test volume. At the same time, the temperature of the optical bench increases slightly because thermal energy can be radiated to deep space less easily. While a larger gold-coated area seems preferable in terms of the temperature of the test volume, it will have to be investigated in more detail how this affects decoherence of quantum superpositions due to the absorption and scattering of blackbody radiation. In particular, the decoherence models we used so far, assumed an isotropic distribution of blackbody radiation. In a precise analysis, it will have to be taken into account that the distribution of blackbody radiation as it is experienced by the quantum system will no longer be isotropic.

In Figure 6, we show the heat flow within the shield structure as well as heat flowing from the spacecraft to the shield structure and heat radiated to deep space. In particular, the inset in the figure shows how quickly the heat flow to deep space diminishes along the sections of the shield, demonstrating that the shield structure is well optimized.

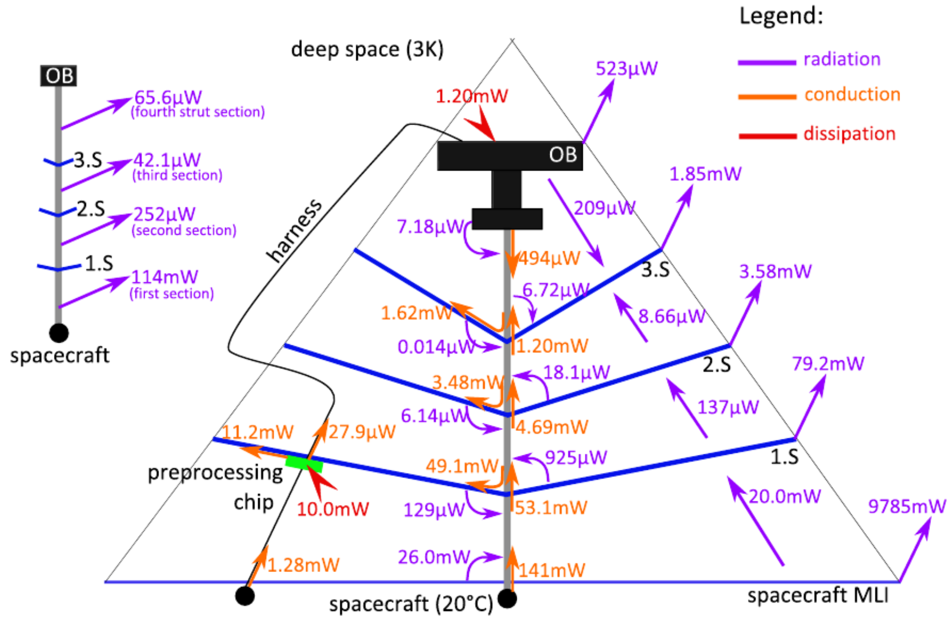

Figure 6: Heat-flow diagram showing conductive and radiative heat transfer as well as sources of power dissipation. The inset on the left-hand side shows the overall radiative heat transfer to deep space from various sections of the shield structure.

A significant part in improving our thermal analysis was to add more elements to our finite-element simulation using ESATAN software. Figure 7 shows, for example, how the number of elements along the struts affects the temperatures predicted by the thermal model. The plots show that a 13-7-3-3 distribution of nodes over the four sections is close to optimal. In particular, a further increase of nodes will only slightly affect the temperature of the optical bench.

Apart from optimizing the optical design and the thermal simulation itself, we also used the opportunity to investigate possible modifications of the shield design. For example, our analysis showed that removing the MLI from the third shield does not affect the temperatures of the test volume and the optical bench. However, removing the MLI from additional shields yielded notable differences (see Table 2).

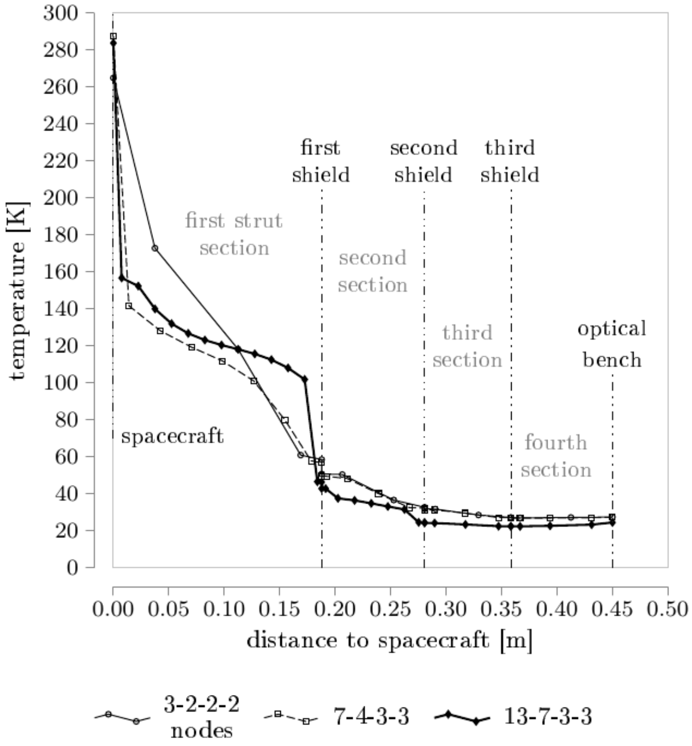

Figure 7: Temperature as a function of the distance from the spacecraft. The plots show the temperature dependence for various numbers of nodes chosen for the four sections.

Increasing the shield size could also be a viable method of further optimizing the achievable temperatures. Corresponding results can be seen in Table 3. Care has to be taken if the diameter of the first shield becomes so large that the shield will receive direct radiation from the sun. In this case, a black instead of gold coating of the shield is preferable to prevent thermal degradation.

Analysis description	test volume [K]	optical bench [K]	3rd shield plate [K]
Base configuration	11.6	24.5	22.3
3rd shield black painted and black MLI outer layer	11.6	24.5	22.4
MLI removed from 3rd shield	11.6	24.5	22.4
MLI removed from 2nd and 3rd shields	11.8	24.6	22.9
MLI removed from 1st, 2nd and 3rd shields	13.0	27.5	26.4

Table 2: Influence of removing the MLI various shields on the temperatures of the optical bench and the test volume.

diameter of the 1st shield [m]	MLI outer layer	test volume [K]	optical bench [K]	outer layer of 1st shield MLI [K]
0.9 (shields not elongated)	gold	11.4	24.5	123.4
2.4 (elongated shields)	gold black	9.7 9.7	18.9 19.1	520.5 370.7

Table 3: Increasing the diameter of the shields can further reduce the temperatures of the test volume and the optical bench.

Different orbital scenarios formed an additional point of interest for our study. In particular, we investigated how long it takes for the optical bench to cool down to temperatures fulfilling the technical requirements of MAQRO (< 20K for the test volume) and how long it would take for the temperature to achieve the steady state after commissioning. Figure 8 shows the respective temperatures as a function of time after commissioning if the spacecraft is at L1 or L2.

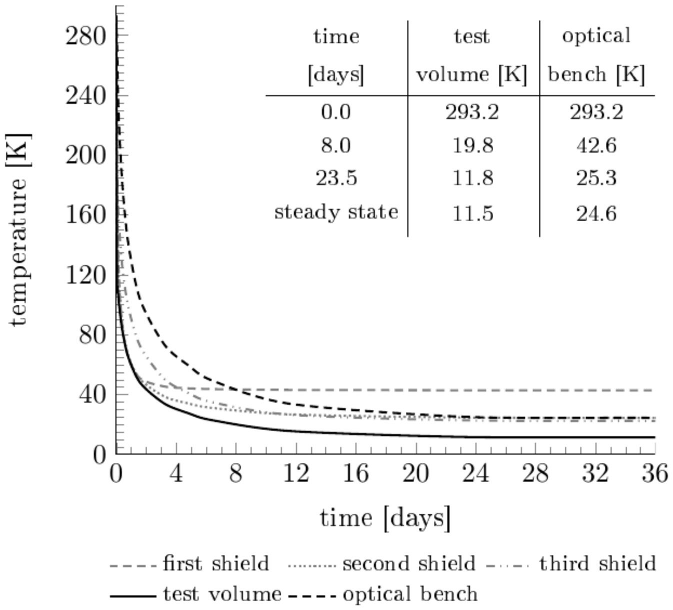

Figure 8: Cool-down of the test volume and the optical bench after commissioning.

As an alternative to an L1/L2 orbit, we investigated the feasibility of a highly-elliptical orbit (HEO). In particular, the orbit we investigated has an altitude of 600000km at apogee, 600km at perigee, with an inclination of 63.4° and an argument of periapsis of 0°. Figure 8 shows that this orbit would only allow for very short periods of time (3 days) around the apogee where the temperatures of the optical bench and the test volume are low enough for MAQRO. However, these periods of time can be extended to about 5 days by using an optical bench of Silicon Carbide (SiC) instead of Zerodur due to the much lower specific heat capacity of SiC.

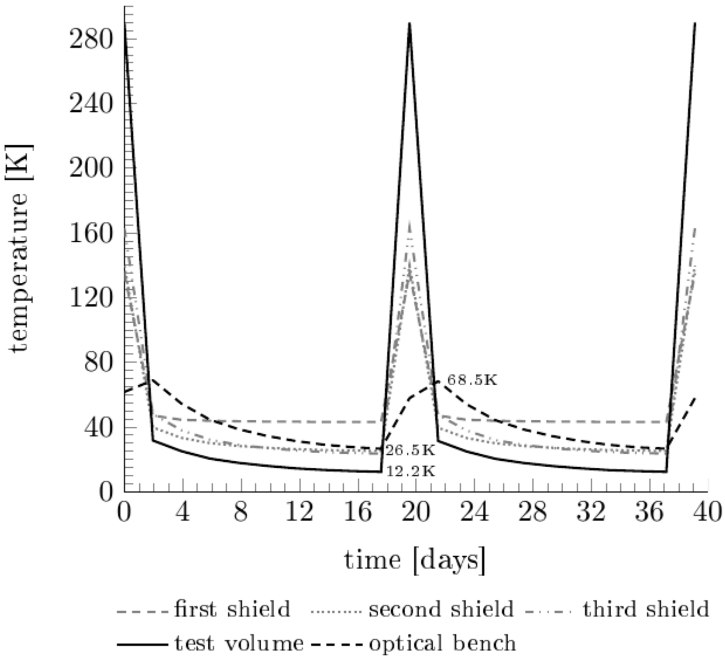

Figure 9: Temperatures as a function of time during for an HEO orbit.

In parallel to this thermal study, we also did another estimation of the vacuum achievable in the vicinity of the optical bench (**WP 2.2**). In particular, we checked earlier results in the course of the original MAQRO proposal. This double-check confirmed our estimate that vacuum levels fulfilling the requirements of MAQRO should be possible for an orbit around L1 or L2. For a HEO orbit, where the shield structure is periodically contaminated by passing by close to Earth's atmosphere would need further investigation. In the case of an L1/L2 orbit, estimates of the interplanetary vacuum indicate that the flow of charged particles originating from the sun should not pose a significant limitation to MAQRO as long as the optical bench points away from the sun. A more detailed analysis of the expected distribution of charged particles from the solar wind around the spacecraft should be performed in the future.

Work package WP 3.1

In **WP 3.1**, we theoretically investigated a novel scheme for 3D intra-cavity cooling of the center-of-mass motion of a dielectric particle. The scheme is an extension of the 1D side-band cooling experiment we recently performed[6]. In this 1D cooling scheme, two TEM_{00} cavity modes were used to trap a dielectric particle and to cool its center-of-mass motion in the *z* direction along the cavity. A central limitation of this setup has been that it only works at relatively high ambient pressures around 1 mbar. This comparatively high pressure results from the method we use for loading nanoparticles into the optical trap. In particular, we load the trap by evaporating a liquid solution containing the nanoparticles with the help of an ultrasonic membrane. By opening a valve, the evaporated liquid containing the nanoparticles is then sucked into the vacuum chamber. This typically results in the pressure inside the vacuum chamber to increase to several 10 mbar and many particles are trapped in the cavity mode. When pumping down, particles get lost from the trapping mode. In this way, it is, in principle, possible to eventually have only a single trapped particle. However, when the pressure goes down to about 1 mbar, all trapped particles are lost. This seems to occur in a critical pressure regime where the particles are heated out of the optical trap [7,8]. In particular, the particles probably escape along the directions *x* and *y* transverse to the cavity mode. Overcoming this limitation in order to achieve 3D trapping at lower pressures is possible by introducing additional cooling mechanisms [9,10]. Trapping in ultra-high vacuum (UHV) is a prerequisite for achieving cooling close to the quantum ground state [6]. While it would, in principle, have been possible to combine our side-band-cooling setup with additional extra-cavity modes for feed-back cooling[9], we chose to take an alternative approach based on using higher-order cavity modes[11]. The advantages of this approach are particularly clear in the case of MAQRO. Instead of adding additional optical components and laser beams to the optical bench of MAQRO, the approach we choose only adds additional modes to the cavity. All elements necessary for generating and controlling these modes can be located within the spacecraft[12].

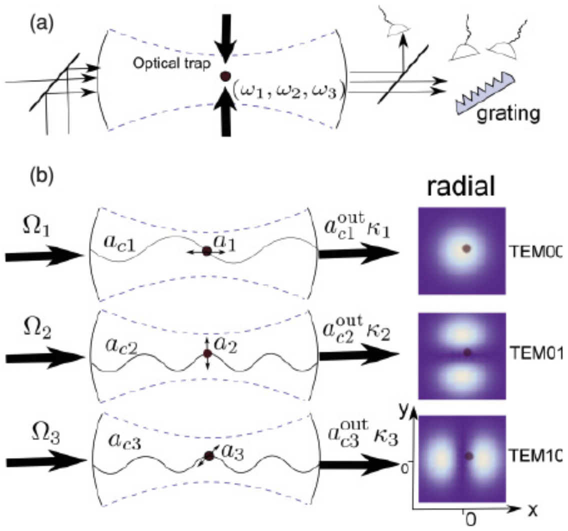

Figure 10: 3D cooling of particle motion as described in Ref. [11]. (a) A particle is trapped by an optical tweezer (black arrows) inside an optical cavity. In addition to the fundamental TEM00 cavity mode, two additional laser beams

(TEM01 and TEM10 modes) are coupled to the cavity The modes can be separately detected in cavity transmission by discerning them in polarization and frequency. **(b)** Illustration of the three spatial mode profiles. Picture taken from Ref.[11].

The approach described in Ref. [11] assumes that a dielectric particle is trapped by a tweezer within a cavity (see Figure 10). The particle introduces a position-dependent shift of the cavity resonance frequency for each of the modes. This frequency shift can be monitored via homodyne measurements of the cavity transmission. One can then generate a feedback signal for modulating the amplitude of the respective modes depending on the particle position. In this way, using the three spatial cavity modes, it becomes possible to implement active 3D feed-back cooling.

Our cooling scheme, which we defined in **WP 3.1**, extends this approach. In particular, our scheme does not rely on optical trapping by a tweezer but the cavity modes themselves are used for trapping. Moreover, our scheme combines the benefits of active feed-back cooling with passive damping in all three modes. A more careful consideration of this approach showed that not using an external tweezer for trapping does not only have benefits. In particular, simply adding TEM_{01} and TEM_{10} modes and independently modulating them according to the motion of the particle does not yield the desired solution. Each of the modes will modify the effective trapping potential, but while the ideal configuration would be for the particle to be constrained to one of the *x-y* diagonals, if both modes have approximately the same amplitude, the effective potential experienced by the particle will be donut shaped with no constraint in the azimuthal direction around the cavity axis. One possible solution would be to also add a TEM_{11} mode but instead, we chose a different approach in order to keep the number of required cavity modes at a minimum. One can overcome this issue by properly choosing the feedback signals for the TEM_{01} and TEM_{10} modes. For the TEM_{01} and TEM_{10} mode, the feedback signals are 2D functions depending on the x and y position of the particle with the gain depending on the intensity of the TEM_{10} and TEM_{01} mode, respectively. This can be used to stabilize the particle on one of the *x-y* diagonals.

From our estimates, the cooling rates achievable in this feedback-cooling scheme should exceed the other dominant sources of friction at high pressures. This should allow us to go the gas pressures low enough such that scattering becomes the dominant source of heating. At this point, it should then be possible to switch off the active feed-back cooling and red detune the three cooling modes in order to achieve backaction cooling. This should allow overcoming the scatter heating and eventually cool close to the ground state.

We are currently preparing to publish the detailed theory of the approach described above. In the laboratory, we first modified our setup in order to implement this cooling approach using our standard cavity (not the bonded one). Later, we designed a completely new vacuum chamber to accommodate the bonded cavity or a more standard cavity plus methods for supplying particles to the chamber in UHV and to load them into the cavity mode. We will describe this setup and our work to implement 3D cooling in the following.

Work packages WP 3.2 and WP 3.3

As the description above shows, in our novel approach to optomechanical 3D cooling, there is no clear distinction between feedback and side-band cooling – they go hand in hand. For this reason, while we originally defined separate work packages WP 3.2 and WP 3.3, we will now discuss them jointly in this subsection.

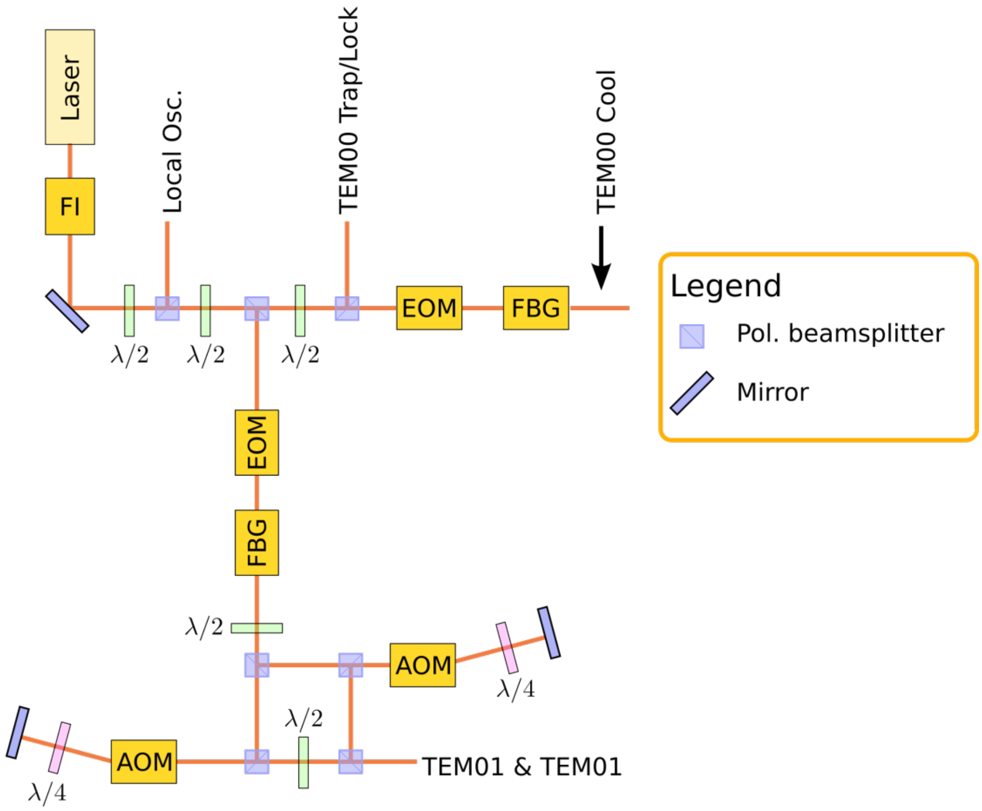

Figure 11: Optical setup for generating the four modes for intracavity trapping and 3D cooling. The fundamental mode of the laser is locked to the optomechanical cavity. The mode for longitudinal cooling is generated using a GHz electro-optic modulator (EOM) & separated from the carrier via a tunable narrow-band fiber Bragg grating. In a similar way, we generate and filter a sideband with a frequency close to the TEM01 and TEM10 modes of the cavity. The precise frequency shift is generated via acousto-optic modulators (AOMs) in double-pass configuration. FI: Faraday Isolator.

Figure 11 shows a schematic of the optical setup used for preparing the four modes for intra-cavity trapping and 3D cooling inside. A Coherent Mephisto (1064nm) is isolated from backreflections via a Faraday Isolator. Part of the beam is split off to form the local oscillator for homodyne measurements. Another part is used for the TEM_{00} trapping mode, which is also used to lock the laser to the cavity via the Pound-Drever-Hall (PDH) technique[13,14]. Two GHz electro-optic modulators (EOMs) in combination with tunable narrow-band fiber Bragg gratings (FBGs) are used to generate sidebands and separate them from the carrier for the cooling TEM_{00} mode and for the

TEM_{01}/TEM_{10} modes. For the higher-order modes, we can use a single EOM because the two modes are relatively close in frequency. To generate two separate modes matching the respective frequencies exactly, we use acousto-optic modulators (AOMs). For feedback cooling, the intracavity amplitude of the higher-order modes can be adjusted by adapting the AOM frequencies.

In order to be able to perform PDH locking of the laser to the fundamental mode, we modulate the TEM_{00} beam with another EOM around 20MHz and monitor the light reflected from the cavity. The two higher-order modes are locked to the cavity in separate PDH circuits. Because the cavity resonance frequencies depend on the particle position, we can use the PDH error signals to determine the particle position in real time & to generate the feedback signal for cooling. In the present setup, this could be achieved with up to 20dB signal-to-noise ratio.

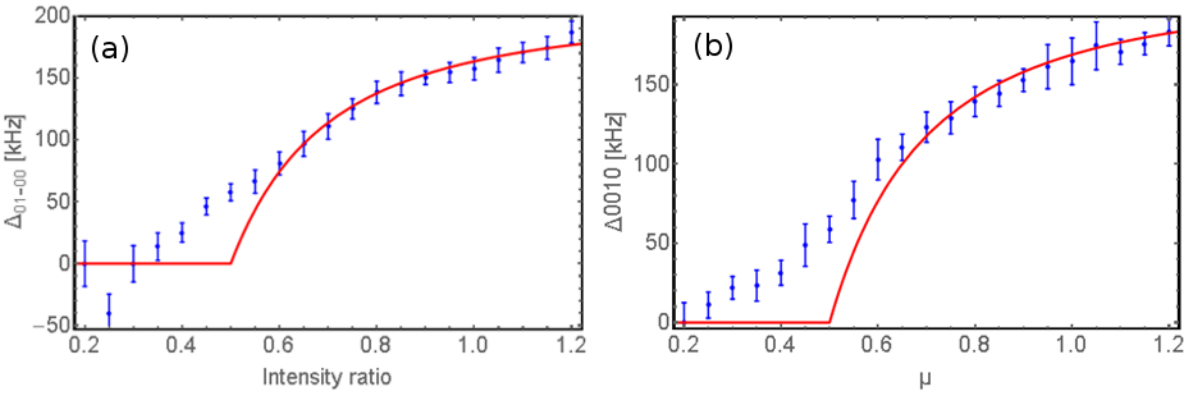

Figure 12: This plots show the action of the higher order modes on the position of a trapped particle. (a) As the ratio μ between the TEM_{01} and the TEM_{00} mode increases, the extremum of the trapping potential shifts from the symmetry axis of the cavity. This leads to a frequency shift in the TEM_{01} and TEM_{00} modes shown on the y axis. (b) This shows equivalent results for the TEM_{10} mode. The red lines represent theoretical predictions.

We show experimental results from this setup in combination with trapped particles in Figure 12. These plots show how a modulation of the intensities of the TEM_{01} and TEM_{10} modes can influence the position of a trapped particle. This is a proof-of-concept demonstration of the feedback method. Given the measured characteristics of the bonded cavity (see below) and its identical geometry to the cavity used in these measurements, the feedback mechanism should work as well with the bonded cavity – possibly better because of its higher stability with respect to temperature fluctuations. Our results on side-band cooling from Ref.[6] were achieved with a near identical cavity geometry. The test setup in relation to the bonded cavity will be discussed below in the context of workpackage 4.3.

A central prerequisite for feedback cooling is the use of fast and low-noise electronic circuitry for generating the feedback signals. For this reason, several of our students worked on novel implementation of PDH locking and the generation of feedback signals using programmable

ARDUINO microcontrollers. For the future, improvements may be possible by using FPGAs instead to benefit from higher bit resolution and bandwidth. This will be discussed in more detail in the master thesis of M. Siegele and the PhD thesis of U. Delic, students of the Aspelmeyer group.

During our work on implementing methods for 3D cooling, new scientific developments led to changes in our optomechanical setup that will have high impact on future optomechanical experiments using optically trapped particles and MAQRO. In particular, one of the central motivations for implementing feedback cooling was to keep the particles stably trapped even at lower gas pressures or even ultra-high vacuum. During the course of the project, it became apparent from results in our group and results in other research groups (in particular, the groups of H. Ulbricht, University of Southampton and the group of P. Barker, University College London[8]) that the particles used in optical-trapping experiments in general had much higher absorption than corresponding bulk material. Because of this higher absorption, the temperature of trapped particles and their thermal energy increase significantly as the pressure of the surrounding gas is reduced[8]. We believe that this is the main reason for particles being heated out of the trap at low gas pressures. In order to investigate this issue, we concluded a series of experiments to determine the grade of cleanliness of nanoparticles from various suppliers and prepared in different ways in our laboratory. We found that quite generally nanoparticles are contaminated with various kinds of organic and inorganic contaminants. By preparing our nanoparticle solutions in a cleanroom environment, using very clean pipettes and solutions (highly clean water or isopropanol), we could significantly reduce the amount of contaminants, and we could reduce the pressure at which trapped particles get lost by more than one order of magnitude.

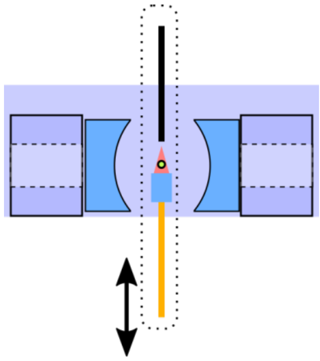

Figure 13: Schematic of the new grin-lens trap for loading particles into the cavity mode. The black line indicates a hollow-core photonic-crystal fiber (HCPCF) used to transport a particle (yellow circle) into the vacuum chamber. A single-mode fiber (orange line) plus a grin lens complete a small tweezer. By tuning the frequencies of the counter-propagating beams, the particle can be transported along the HCPCF and trapped between the grin lens and the HCPCF tip. This whole setup is placed on a translation stage to align it with the cavity mode in the bonded cavity.

In addition, we decided to integrate a novel loading mechanism with our optomechanical setup in order to supply cleaner particles to our trapping mode, to avoid contaminating our cavity mirrors and the vacuum chamber as well as to increase the technological readiness towards MAQRO. In particular, the contamination of our cavity mirrors was a central worry with respect to the bonded cavity. While it is possible to exchange cavity mirrors in a standard cavity holder when they get contaminated, this is not possible in a bonded cavity. Given our old loading mechanism, a large quantity of particles and liquid was sucked into the vacuum chamber. Eventually, this would have led to particles and residues of the carrying solution to cover the cavity mirrors of the bonded cavity. For this reason, we decided to integrate our optomechanical setup with a cleaner loading mechanism before inserting the bonded cavity into the setup.

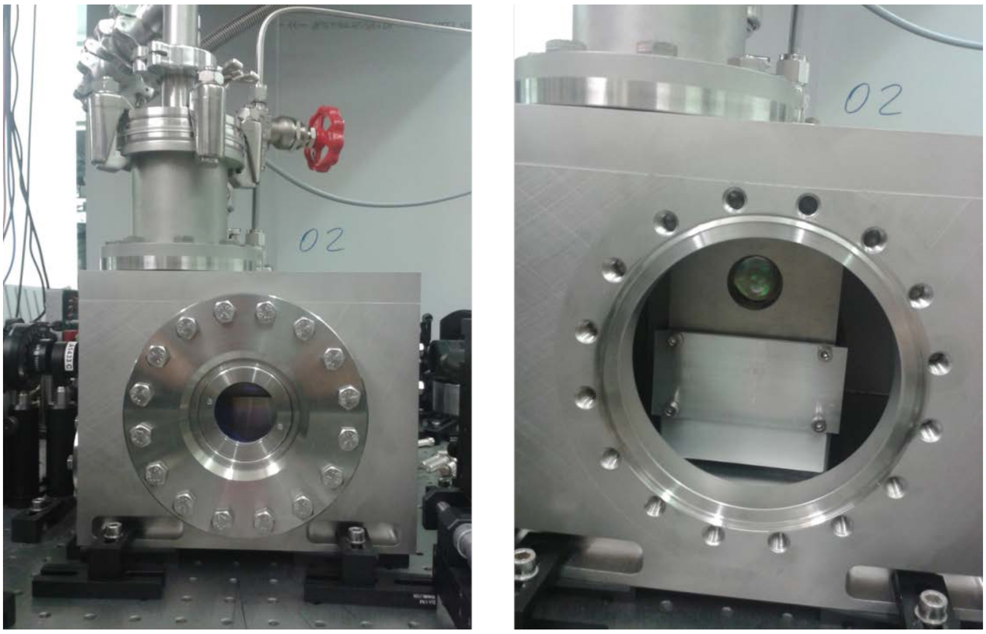

Figure 14: The new vacuum chamber. (left), closed chamber showing the view port. (right), open chamber showing the cavity holder plus two metal blocks beneath used to mount the cavity holder.

To this end, we devised a scheme where particle can be transported along a hollow-core photonic crystal fiber and then trapped between the tip of that fiber and a grin lens focusing light counterpropagating through a single-mode fiber (see Figure 13). This small trap can be put on a translation stage to position it with respect to the mode of the bonded cavity inside the vacuum chamber. In order to integrate this scheme with the existing optomechanical setup, we designed a new vacuum chamber (see Figure 14) that can hold the translateable grin-lens trap as well as our high-finesse cavity. For first tests, we used a standard, metal cavity holder. In order to allow tests with the bonded cavity and with the grin-lens loading mechanism independent of the optomechanical setup, we duplicate vacuum chamber was built as well as a metal cavity with the same dimensions as the bonded cavity. Unfortunately, a mistake occurred in the design of this metal cavity as well as the corresponding cavity holder and its geometry was different from the bonded cavity. For this reason, we could not complete these tests within the reporting period. We are currently in the process of redesigning the cavity holder in order to perform tests with the grin-lens trap and the bonded cavity. We will implement a second bonded test cavity with even higher finesse for additional tests. This work will be completed only after the reporting period.

Work package WP 4.1

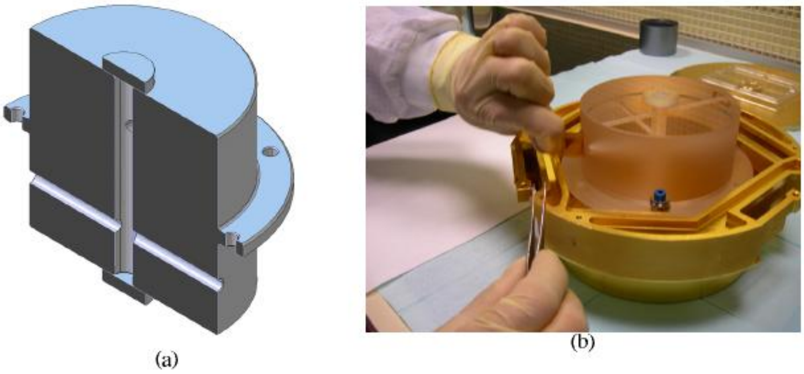

Figure 15: Implementation of a stable cavity by gluing mirrors to both ends of a block of low-thermal-expansion material. A hole is drilled through the block to accommodate the optical cavity mode. Picture from Ref.[15].

A central goal of MAQROsteps has been to increase the TRL of cavity technology to be used in MAQRO. In particular, we aimed at designing and implementing a stable, space-proof cavity design and to test its applicability in a laboratory environment. For this purpose, we investigated possible approaches for realizing a cavity design where high-finesse cavity mirrors are glued to Zerodur. In a room-temperature environment as in our lab, Zerodur has a very low thermal-expansion coefficient, promising the feasibility of implementing a highly stable cavity. Typically, stable cavity designs are implemented by gluing mirrors from both ends to low-thermal-expansion spacers with a hole drilled through them to allow for the unimpeded passage of the cavity mode (see Figure 15 and Refs. [15,16]). However, such a cavity design could not be implemented in our case because (1) it restricts the optical access to our trapped particle and (2) it impedes passive cooling of the test volume because it would be surrounded by comparatively hot material.

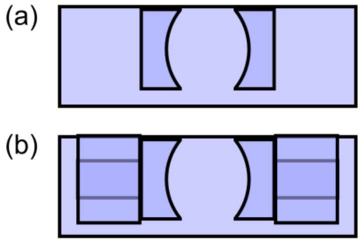

Figure 16: Designs for a stable cavity with freely standing mirrors. **(a)** Original concept of directly bonding the mirrors to a baseplate. **(b)** Improved design where each mirror is glued to a freely standing spacer.

Instead, our original idea was to directly bond or glue high-finesse cavity mirrors to a baseplate of low-thermal-expansion material (see Figure 16(a)). Especially for a long cavity as in MAQRO (cavity length: 97.5mm), such a cavity design results in a large solid angle of deep space surrounding the test volume. While hydroxide-catalysis bonding[17] would, in principle, have been a viable option for implementing such a design, this technique places very stringent limits on how long the bonded elements can still be adjusted once they are placed. The short time-span for aligning the optical elements may prove a significant restriction in the case of implementing a high-finesse cavity. Adhesive bonding[18] provides an attractive alternative because it significantly relaxes that time constraint. Moreover, using adhesive bonding provides the opportunity of finding a good approach for implementing such a cavity design without the additional time constraint. Our implementations of adhesively bonded cavity designs may then be seen as a precursor for a possible future cavity design using hydroxide-catalysis bonding.

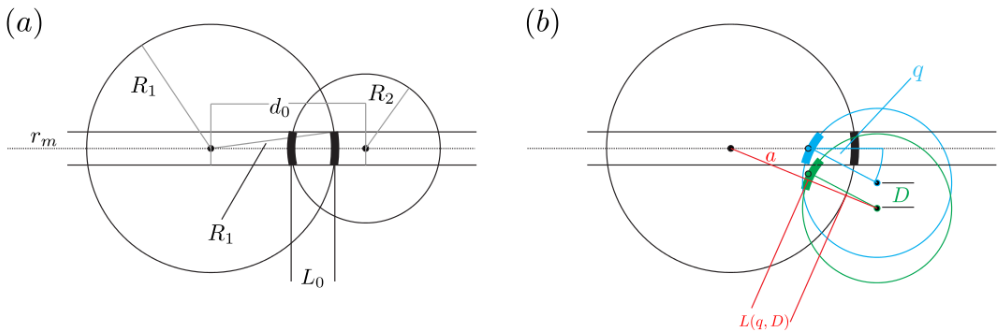

Figure 17: Geometrical considerations for determining the tolerances for the design of a bonded cavity. **(a)** Base cavity design. L_0: cavity length; R_1, R_2: radii of mirror curvature; d_0: distance between the two circles defining the mirror surfaces: r_0: radius of the mirror substrate. **(b)** One mirror is displaced by D and tilted by an angle q with respect to the other. The schematic illustrates the resulting new cavity length L(q,D) and the angle α.

However, our original idea for the cavity design as illustrated in Figure 16(a) proved to have a significant drawback: the center of the curved surface of the mirror typically is only defined with an accuracy of 0.1mm by the manufacturer. To allow achieving higher accuracy in the positioning of the mirrors, we modified our intended design as depicted in Figure 16(b). The general idea was that, at first, spacers with a center hole drilled through them are placed on the baseplate. Only later, the cavity mirrors were to be bonded to the spacers. This approach should allow for precise positioning of the mirrors along the surface of the spacers.

In order to clearly define the design for the bonded cavity, we had to analyze how well we would have to position the cavity mirrors, and how well the respective optical elements would have to be fabricated. That means, we had to define what the tolerances would be for our cavity design. In particular, we decided to investigate this for two different designs. On the one hand, we wanted to implement a cavity design that would replace the existing standard cavity in our laboratory experiments on trapping and cooling dielectric spheres. On the other hand, we wanted to implement a cavity design with the parameters of the cavity as needed for MAQRO. For the first cavity, the design parameters were: 13mm cavity length and a finesse of 10^5. For the second cavity, we wanted to have a cavity length of 97.5mm and a finesse of at least 3×10^4. In both cases, we planned using spherical cavity mirrors with a substrate radius of ¼ inch. For the first cavity, this choice was based on the already existing cavity setup in our laboratory because we wanted to implement a test cavity as close to the one in our existing setup as possible. For the second cavity, the size of the mirrors seemed optimal because they are large enough to easily avoid clipping of the cavity mode and also to allow some tolerance in the orientation of the cavity mode. On the other hand, we did not want to use larger mirrors because one of the goals of the MAQRO cavity is of course to achieve a maximum of solid angle of view with deep space for passive cooling.

Because of the spherical cavity mirrors, theoretically, it is still possible to form a stable cavity even for large displacements of the mirrors and angles between them. But, in this case, the cavity mode will also be displaced with respect to the mirror centers. If one takes into account the finite size of the mirrors and the cavity mode at the mirrors, this provides a natural limitation of relative angles and displacements of the mirrors because eventually the cavity mode will be clipped at the mirror edges. Moreover, the cavity length will be different from the ideal cavity. This is illustrated in Figure 17.

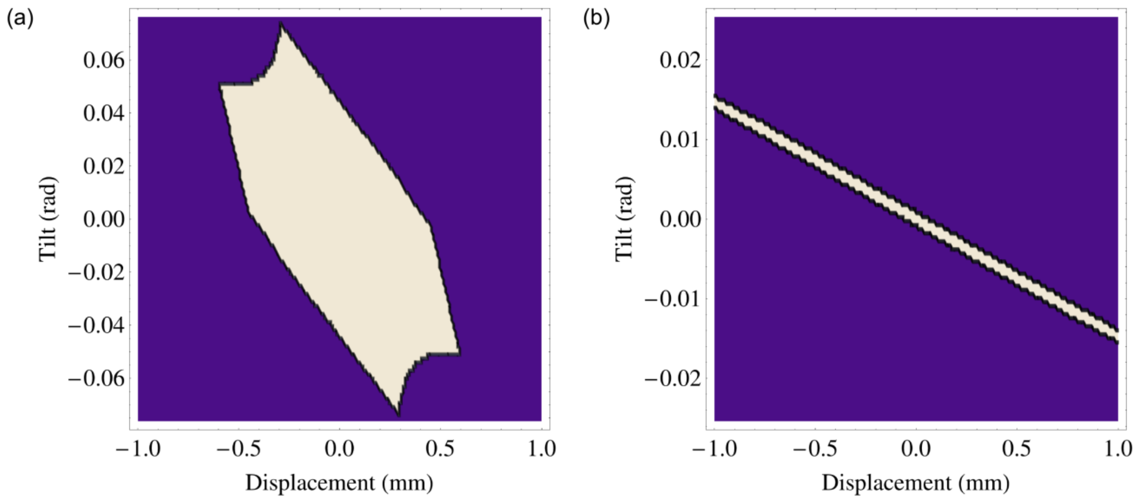

Figure 18: Design tolerances. The bright regions represent the allowed parameter range or relative mirror tilt and displacement. **(a)** Design tolerances for the lab cavity. **(b)** Design tolerances for the MAQRO cavity.

In particular, we consider a cavity that ideally has a cavity length L_0 and is formed by two mirrors with radii of curvature R_1 and R_2, and both with a substrate radius of r_0. Now, if one mirror is displace with respect to the other by a distance D and tilted with respect to it by an angle q, then a stable cavity mode will be possible at an angle α with respect to the ideal cavity mode and with a new cavity length, $L(q, D)$, as shown in Figure 17(b). In order to determine the tolerances of the design, we assume that we will not clip the beam if the point where the new cavity mode hits the mirror is at most $\frac{r_0}{10}$ from the center of the mirror, and if the new cavity length is different from the old one by at most by 0.1%. These the limit on the displacement is chosen conservatively and will, in our case, safely prevent any beam clipping at the mirror edges. The change in cavity length by a maximum of 0.1% ensures that the effective cavity geometry is close to the intended one.

Figure 18 shows the resulting design tolerances for the lab cavity and for the MAQRO cavity. For the lab cavity, we the relative displacement of the cavity mirrors should be at most on the order of 0.1 mm, and the relative angle should be at most on the order of 10 mrad. These are relatively relaxed requirements. In the case of the MAQRO cavity, on the other hand, the tolerances are more stringent by approximately one order of magnitude. For this reason, we chose first to implement the lab cavity to gain experience using the adhesive bonding procedure and because this cavity could be directly compared with the existing, standard cavity setup. These considerations and a detailed design of the components necessary for our cavity designs concluded **WP 4.1** of this project.

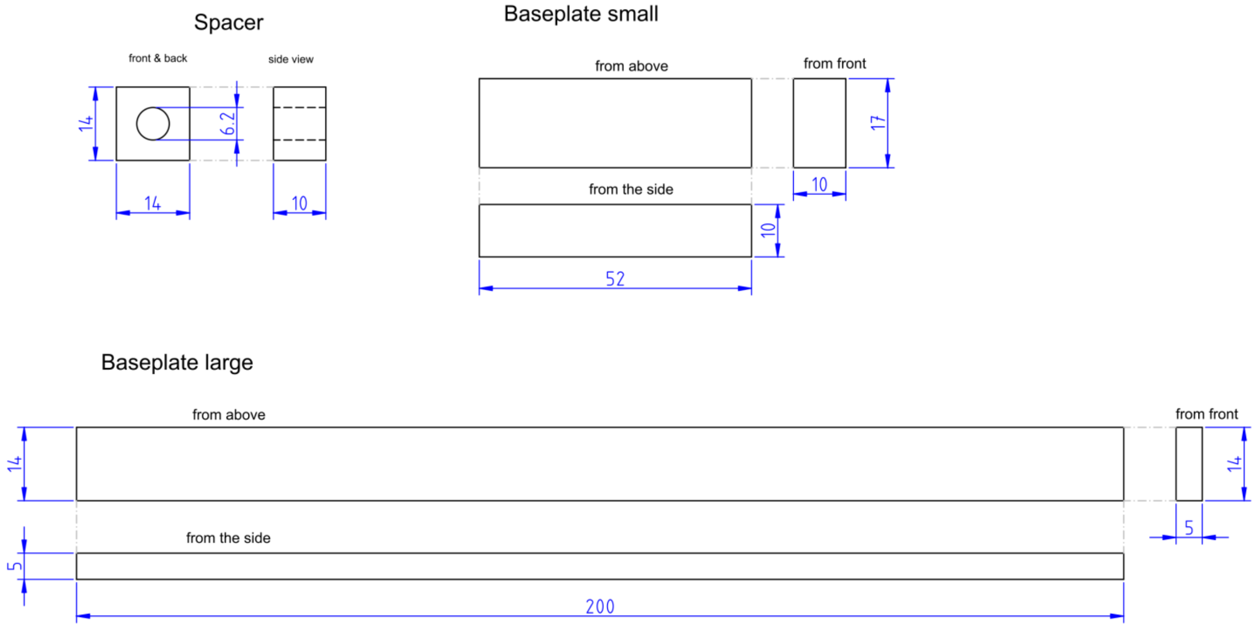

Figure 19: CAD Drawings of the Zerodur components for the cavity designs. All dimensions are given in mm. The lab cavity consists of the small baseplate plus two spacers for the cavity mirrors. The MAQRO cavity consists of the large baseplate and three spacers – two for the cavity mirrors plus one spacer for a plano-convex lens to match the incoming beam to the cavity mode.

Work package WP 4.2

As a first step towards implementing our cavity designs (**WP 4.2**), based on the tolerances calculated, we placed an order for Zerodur baseplates and spacers as shown in Figure 19 for the two cavity designs. We ordered enough components to suffice for two implementations of the lab design and for two implementations of the MAQRO design. This was to ensure that we would not have to order new components should the bonding procedure fail. Moreover, this will allow for testing the reproducibility of our design procedure, and for testing and using the designs in parallel in multiple test setups.

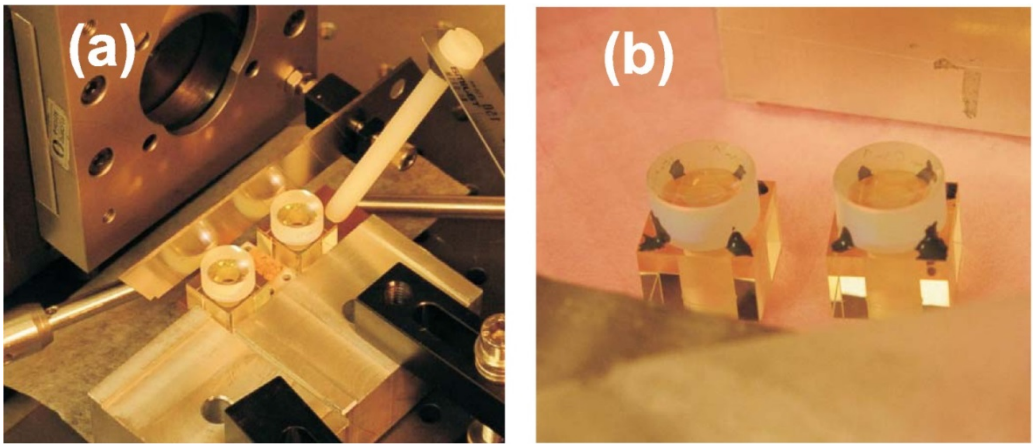

Figure 20: Adhesive bonding of cavity mirrors. (a) Positioning two cavity mirrors on top of cavity spacers. The image shows the positioning arms, clamps, reference surfaces and a translation stage used to position the mirrors on the spacers. **(b)** Close-up of the finished components. The black spots are Hysol 9361 glue from Loctite.

Because the implementation of a bonded optical setup does not allow for later realignment of the components, we had to define a very clear procedure for implementing the lab cavity before proceeding with bonding the optical elements. In particular, based on the design tolerances, we decided that it would be best to first bond the mirrors to the spacers as shown in Figure 20. Only in the next step, the spacers with the mirrors were bonded to the baseplate as shown in Figure 21.

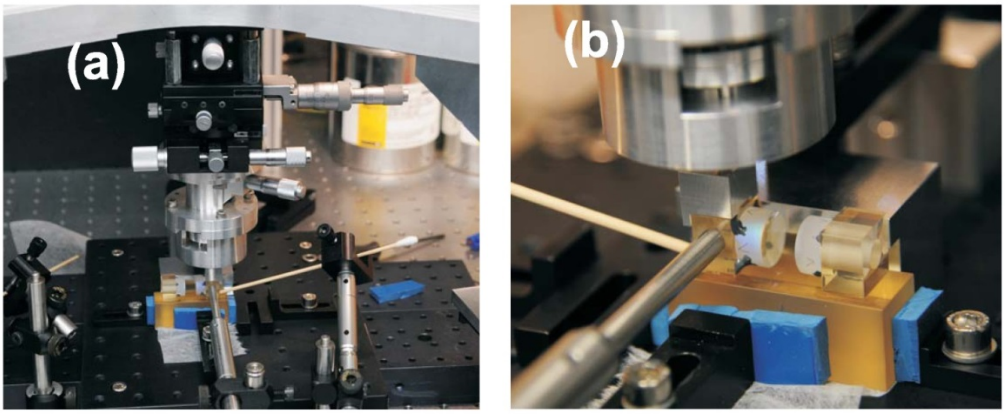

Figure 21: Adhesive bonding of the mounted mirrors to the baseplate. (a) Picture of the combination of translation stages, positioning arms and clamps to position one of the mounted mirrors. **(b)** Close-up picture showing the mounted mirrors on top of the clamped baseplate.

This was made possible by the relaxed tolerances for the lab cavity. In particular the inaccuracy of 0.1mm in the position of the center of the curved mirror surfaces is within the design tolerance for the lab cavity. Instead of using only the space-proof glue Hysol 9313 from Loctite[18], we also used a second sort of space-proof glue, Hysol 9361 from Loctite. We used Hysol 9313 for adhesively bonding the spacers to the baseplate, and we used Loctite 9361 for adhesively bonding the cavity mirrors to the spacers. The reason for using Loctite 9361 for the cavity mirrors was that it does not spread as widely over the bonded surfaces. This reduced the risk of glue covering the open apertures on the flat sides of the cavity mirrors. We chose to apply the glue at four equally spaced spots around the mirror circumference (see Figure 20). Once the mirrors were fixedly bonded to the spacers, the spacers were glued to the baseplate using Hysol 9313. This type of glue forms a very evenly distributed, thin layer (several µm) of adhesive between the bonded surfaces.

In our test setup for characterizing the finesse of the finished cavity, we mounted the cavity in an ultra-high vacuum chamber with optical access from the left and the right in Figure 22. The vacuum chamber was operated at a pressure of about 10^{-6} mbar. We did not observe any notable degradation of the vacuum quality due to the adhesive used for the cavity.

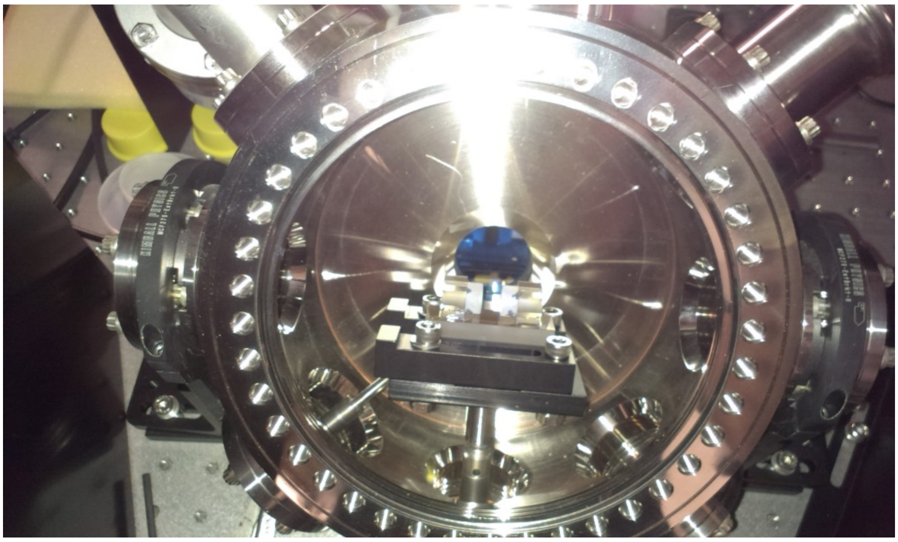

Figure 22: Lab cavity mounted in vacuum chamber.

In our optical test setup (see Figure 23), we locked a 1064nm laser (Mephisto 500NSE) to the cavity using Pound-Drever-Hall (PDH) locking[13,19]. In order to generate an error signal for PDH locking, we modulated the laser beam with an electro-optic modulator (EOM) at approximately 18MHz. After passing a fiber polarizing beam splitter (PBS), the light was set to right-hand circularly polarized light using a combination of $\frac{\lambda}{2}$ and $\frac{\lambda}{4}$ waveplates. This allows separating the light reflected from the cavity from the cavity input at the fiber PBS. That reflected light is then detected, and the signal is multiplied with the same signal used to drive the EOM. The resulting signal is passed through a low-pass filter before being fed to a PID (proportional-integral-derivative) circuit to generate the error signal for PDH locking.

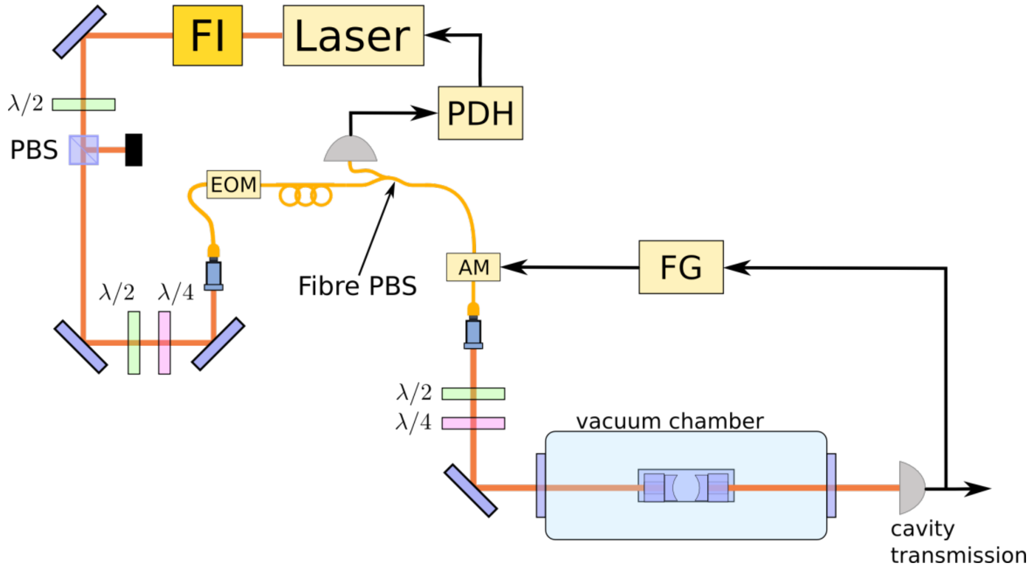

Figure 23: Optical test setup. We locked a laser to the bonded cavity via Pound-Drever-Hall (PDH) locking. The cavity finesse was determined by a cavity-ring-down measurement. For details, see the main text.

The cavity transmission was detected using a fast photo diode, and the resulting signal could be observed on an oscilloscope. Part of that signal could be used to trigger a function generator (FG) to produce a rectangular pulse whenever the cavity transmission surpassed a given threshold. Using these pulses, we could switch off the cavity input field using an amplitude modulator (AM). In this way, it was possible to observe the cavity ring down and to determine the cavity finesse. A representative signal trace and an exponential fit to the ringdown are shown in Figure 24. We performed four measurements of that type and got an overall result of $\mathcal{F} = (98 \pm 2) \times 10^3$ for the cavity finesse, agreeing well with the aimed-for finesse of 10^5.

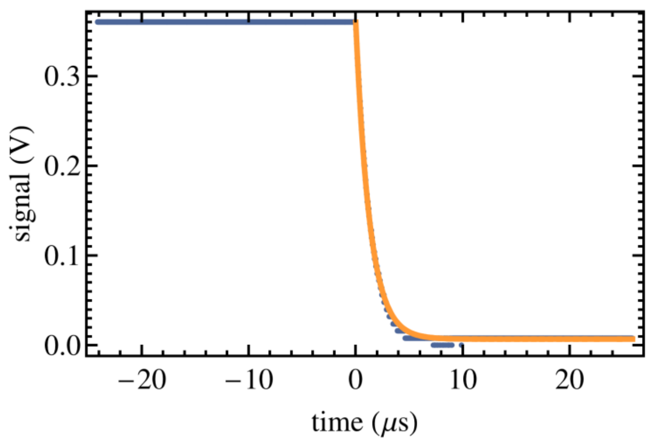

Figure 24: Cavity ringdown measurement. The blue dots represent the photo-diode signal of the cavity transmission. The cavity input is switched off at $\boldsymbol{t = 0\ \mu s}$ resulting in an exponential decay of the intra-cavity field. The orange line is an exponential fit – it was chosen to begin at the position of the maximum negative derivative of the signal.

In the second reporting period, we repeated the ringdown measurements in an improved approach. We decided to do so in order to collect more data for the publication in preparation. In particular, we fully characterized the reflected and transmitted beam at various points of the setup, and we performed ringdown measurements for the light reflected by as well as transmitted by the cavity. The resulting data will be part of the paper in preparation. For the improved ringdown measurements, instead of triggering the cavity ringdown on the detection of the transmitted light, we chose to periodically switch off the cavity input via a rectangular waveform supplied to the amplitude modulator. We chose the repetition frequency of the switch-off to be $10\ \mathrm{Hz}$ so we could collect enough ringdown traces within a reasonably short time. The duration of the switch-off was $67\mu\mathrm{s}$. This time was longer than the ringdown time but short enough for the cavity lock to remain stable. Fits to the ringdown in the transmitted light yielded a cavity finesse of $\mathcal{F}_t = (91 \pm 2) \times 10^3$. For the reflected light, the situation is slightly more complicated. When the input light is switched off, the reflected light starts to drop quickly because not all light is coupled into the cavity. The light that is simply reflected drops immediately, the speed being limited by the detector response. After some time, the slower cavity ringdown takes over. Because of slight inaccuracies in determining the point where the transition from one to the other decay occurs, the error in the resulting finesse is larger than in the transmitted case. We arrive at a finesse of $\mathcal{F}_r = (94 \pm 5) \times 10^3$. This is compatible with $\mathcal{F}_t$ above. However, there is a slight discrepancy between $\mathcal{F}_t$ the finesse determined using by triggering on the transmitted light. We will have to investigate this discrepancy before publishing our results.

This concludes **WP 4.2**, in principle, but we continued implementing the cavity representative for the cavity geometry planned for MAQRO, and we plan to implement one more lab cavity and a further improved version of the MAQRO cavity in the future. The corresponding efforts and plans will be described below. However, the experiments on feed-back and cavity cooling will be performed using the lab cavity already implemented and described here.

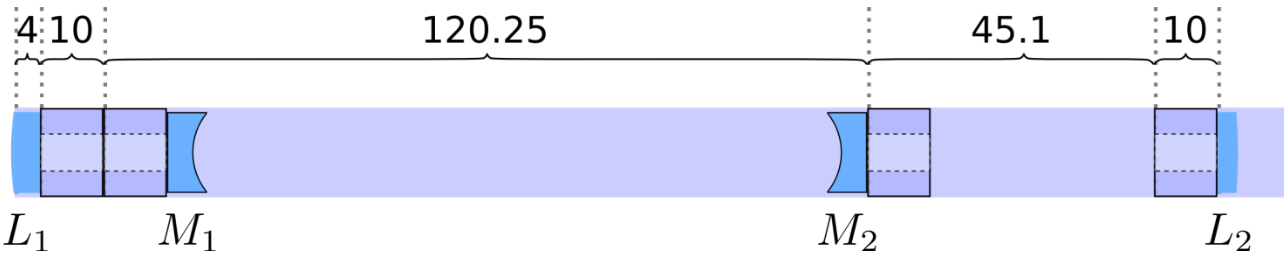

Figure 25: Geometry of the MAQRO cavity implemented. The spacers ($\mathbf{14} \times \mathbf{14} \times \mathbf{10}\mathrm{mm}^3$) with their central clearance holes are shown as gray rectangles. The gray square in the background illustrates the top view of the baseplate ($\mathbf{200} \times \mathbf{14} \times \mathbf{5}\mathrm{mm}^3$). $\boldsymbol{L}_{\mathbf{1,2}}$ are plano convex lenses, $\boldsymbol{M}_{\mathbf{1,2}}$ represents the spherical cavity mirrors. The numbers are distances in mm.

The bonding of the first lab cavity could be conducted at the facilities of Airbus D & S only using mechanical and no optical references for alignment. For bonding a MAQRO cavity, the angle tolerances were significantly more restrictive (see Figure 18), requiring optical reference beams. For this reason, we decided to implement the MAQRO cavity designs in our laboratories at the University of Vienna. Assembling the MAQRO cavity was more challenging than in the case of the lab cavity because of the more stringent constraints on the fabrication and alignment tolerances. While the Zerodur components for the MAQRO cavity have been fabricated according to these stricter requirements, using only mechanical means for positioning the optical components would not have provided sufficient accuracy. Instead, we had to use optical means to achieve the required accuracies.

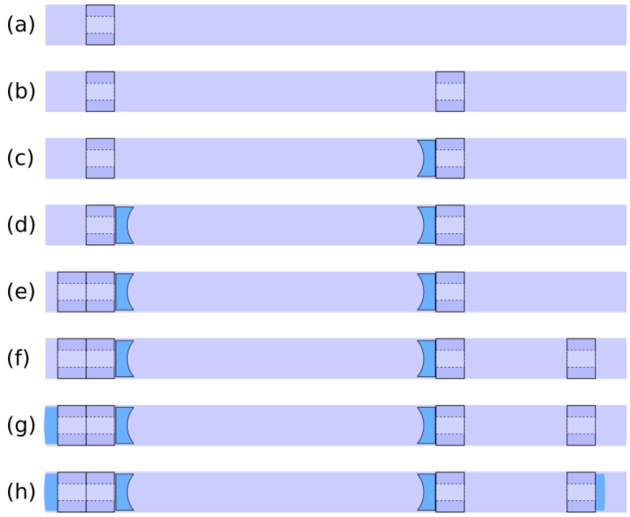

Figure 26: Steps of one-by-one placing the various elements on the baseplate. Always bonding and aligning the spacers first provides the possibility of restricting the possible movements of the optical elements to the plane parallel to the spacer surface.

The final design of the MAQRO cavity implemented is shown in Figure 25. So far, only the spacers holding the cavity mirrors as well as the cavity mirrors $\boldsymbol{M}_{1,2}$ were bonded. Shortly after the reporting period we intend to complete the implementation. In the following, we will describe the alignment procedure used so far, and how we will complete the implementation of the cavity. Figure 26 illustrates the individual steps in implementing the MAQRO cavity. So far, steps (a) to (d) have been realized. For the optical alignment, we implemented and used the setup outlined in Figure 27.

For alignment, we use 532 nm light from a Coherent Verdi V10. This wavelength was chosen for two reasons – on the one hand, it allows easy alignment because the light is visible to the naked eye, and beams of that wavelength diverge more slowly than comparable beams of 1064 nm light. We coupled light into two single-mode fibers in order to be able to shine light at the cavity from two directions.

After exiting their respective fiber couplers the two beams are collimated in order to generate well collimated beams with about 1mm diameter over a distance of 4m or more. This way, small angular deviations of beams on the order of one arc minute could be resolved easily by eye after a distance of 3 to 4 meters.

The optical setup worked as follows: the single-mode fiber couplers for two beams were aligned such that light from one coupler was coupled well into the other coupler. This assured that the two counterpropagating beams were well overlapped. To generate reference beams for later precision alignment and to compare them with light reflected from optical elements in the optical-cavity setup, on each side we used two $\lambda/4$ waveplates in combination with a polarizing beamsplitter cube. Moreover, this allowed adjusting the relative intensity between back reflections and the reference beam.

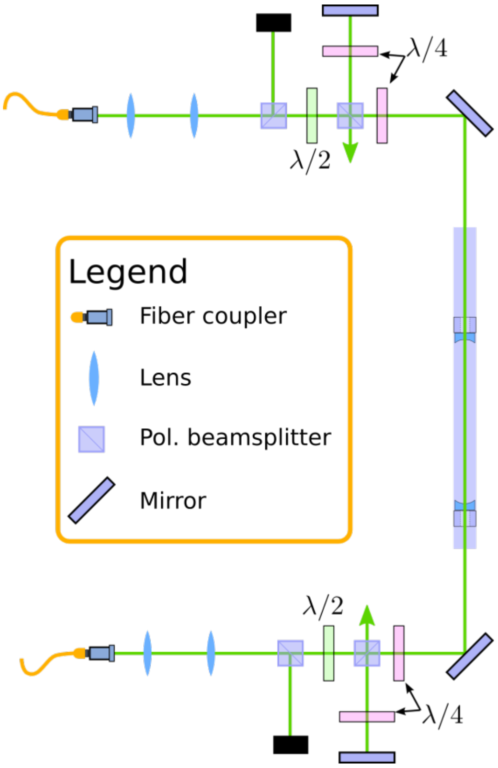

Figure 27: Setup for optically aligning the elements for bonding on the baseplate. Details of the setup and its use are described in the text. $\lambda/2$ waveplates are used to adjust the intensities of two beams passing towards the cavity. On each side two $\lambda/4$ waveplates are used to adjust the intensity of backreflections from the cavity and the intensity of a reference beams used for alignment. The black rectangles are beam blocks.

As a first step of alignment, we made sure that the two counterpropagating beams were parallel to the optical table top and that the beam path was parallel to the mounting holes of the table. Next, we mounted the baseplate of the MAQRO cavity on translation stages to allow translation in the two directions perpendicular to the beam path – one in the “x” direction parallel, the other in the “y” direction perpendicular to the table top. We denote the direction of the beam as “z”. Moreover, we used a tilt platform to be able to tilt the baseplate around the “x” and the “z” direction. By additionally rotating the overall mounting platform around the “y” axis by hand, we could align the baseplate such that the backreflections from both of its end faces were overlapped with the reference beam with accuracy significantly better than 2 arc minutes. The baseplate was fixed between metal clamps thicker than the baseplate itself. This also provided guiding for spacers put on the baseplate.

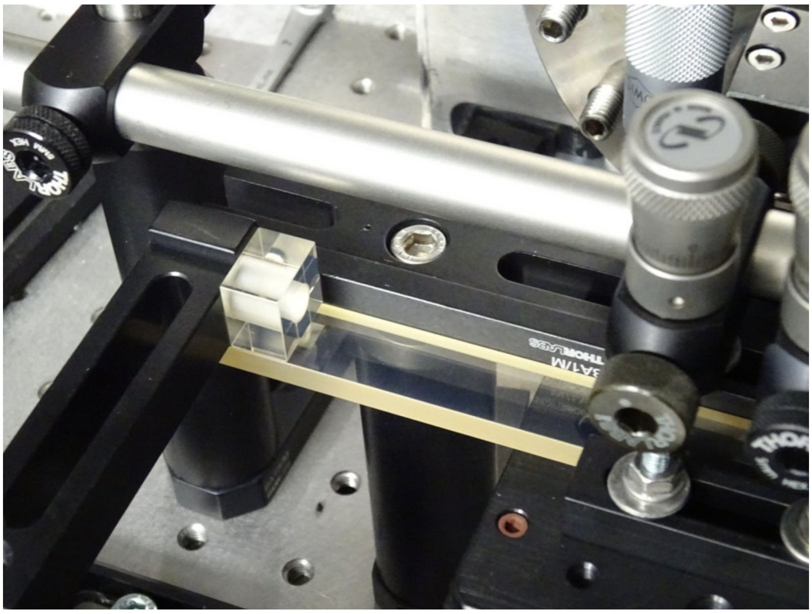

Figure 28: Spacer for $\boldsymbol{M_1}$ positioned on the base plate using a metallic clamp for defining the position of the spacer along the baseplate and a metallic base on the side to guide the motion. On the right-hand side, the picture shows two actuators mounted atop the baseplate. These were used later to press the glued spacer against the baseplate.

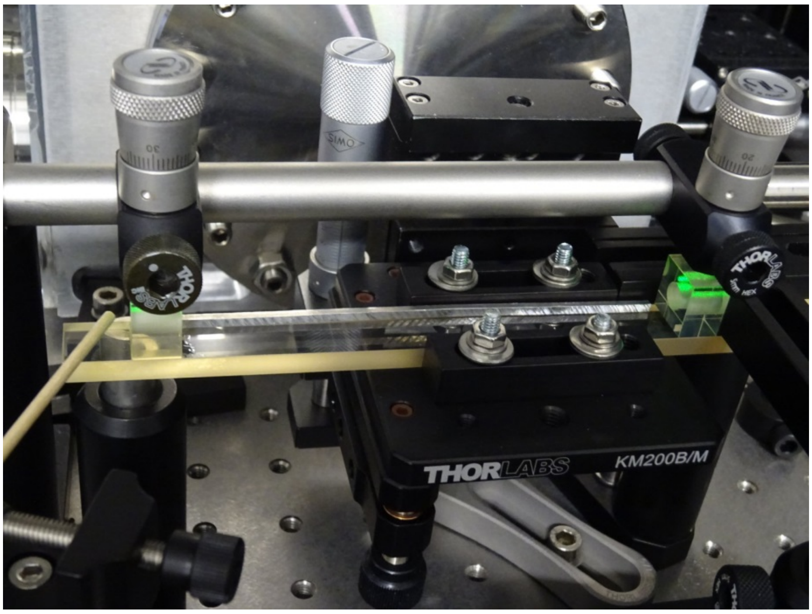

Figure 29: The picture shows the actuator holding the spacer in place and the wooden stick of a cotton-tipped applicator attached to a translation stage (not shown) for precision tilting of the spacer around the "y" axis.

In order to realize step (a) of Figure 26, we put a spacer on the baseplate and translate the whole baseplate in the "y" direction such that the laser beam hit the spacer above the clearance hole. This provided a clear backreflection to compare with the reference beam. In order to position the spacer at the intended position along the "z" direction along the beam, we used another metal clamp on top of a translation stage for movement along "z". This clamp was originally aligned to be parallel to the front face of the base plate. Then it was moved by 4mm along the “z” direction. To define the position along the long edge of the baseplate, we mounted a metal post base next to the baseplate (see Figure 28). Finally, we mixed the two components of Hysol 9313 glue from Loctite and used a pipette tip to supply a thin sheet of glue to the side of the spacer to be glued to the surface. Next, we touched the glued face of the spacer to the baseplate at the position defined by the metal spacer and baseplate positioned earlier. To hold the spacer in place, we pressed it against the baseplate using an actuator mounted above the baseplate (see Figure 29).

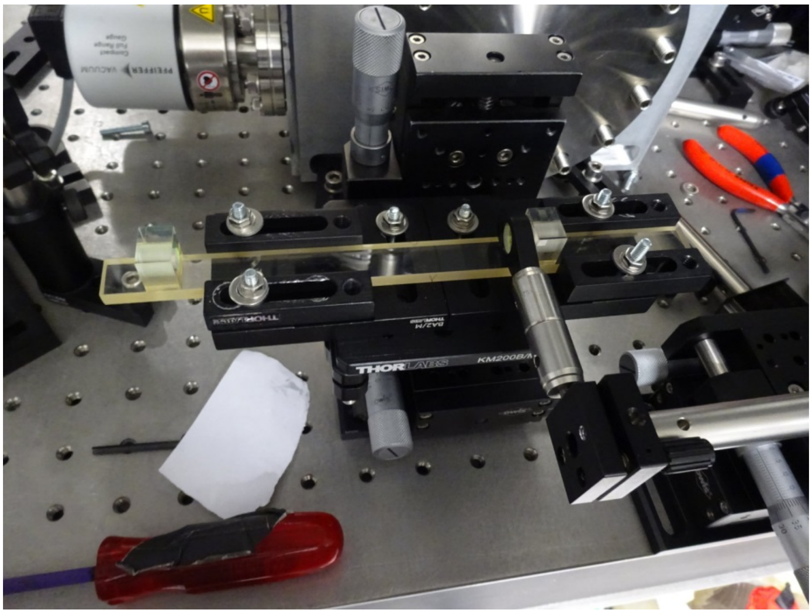

Figure 30: We used a mirror mount on a 2-axis tilt and 3-axis translation stage to position mirror $\boldsymbol{M_2}$ against its spacer.

We used an additional translation stage with a cotton-tipped applicator attached such that the wooden stick touched the spacer edge. By translating this cotton-tipped applicator we could precisely adjust the angle of the spacer front face around the “y” direction. Further fine adjustments could be made by hand while the spacer was held against the baseplate.

To define the distance between this first spacer and the spacer for $\boldsymbol{M_2}$, we had a thin piece of metal made that was slightly shorter than the intended length. Then we again used the combination of a baseplate for guiding and a metal clamp on a translation stage to fine tune the position of the spacer. After that, we repeated the same procedure for gluing the spacer for $\boldsymbol{M_2}$, except that we used two cotton-tipped applicators on translation stages for fine adjustments. This completed step (b) of Figure 26.

Next, we used an “xyz” combination of translation stages plus a tilt platform for rotations around “x” and “y” for positioning $\boldsymbol{M_2}$. We first used the backreflection from the flat side of the mirror to assure the mirror’s symmetry axis was parallel to the beam. Then we looked at the transmitted beam. It created a round halo due to refraction at the curved mirror surface. We could then center of the mirror’s curved surface on the beam by looking at this halo with respect to the counterpropagating beam. Once this was done, the mirror could be moved away from the spacer surface along the “z” direction. We then used our pipette tip to put small droplets of glue at four positions around the spacer clearance hole.

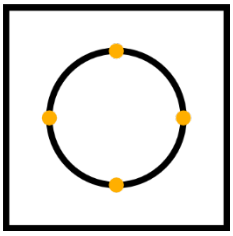

Figure 31: The orange dots indicate where we positioned the glue on the spacers for bonding the mirrors.

As soon as the adhesive was applied, we moved the mirror back against the spacer along the “z” direction. While doing this, we monitored the backreflection from the flat backside of the mirror with respect to the reference beam. Tilting the mirror mount allowed to overlap the backreflection with the reference beam. In addition, we again checked the relative position of the halo of the beam transmitted through the mirror and used “xy” translation to center it on the counterpropagating beam. Once this was done, we left the mirror in position for the adhesive to cure. After the curing of about 8 hours, we double-checked the alignment to assure that the curing had not altered it.

For the mirror $\boldsymbol{M_1}$, the situation was a bit more difficult because there were no unaltered counterpropagating beams left. To overcome this issue, we place a mirror between the two spacers in order to reflect the incoming beam. The mirror was aligned such that its reflection overlapped the reference beam. From there, the alignment procedure for $\boldsymbol{M_1}$ was equivalent to that of $\boldsymbol{M_2}$.

Unfortunately, we could not finish the remaining steps in Figure 26 during the reporting period. We will add the lenses, characterize the cavity and aim at publishing the results as soon as possible.

Work package WP 4.3

As we described earlier with respect to workpackages WP 3.2 and WP 3.3, our first experimental results on the feedback mechanism as well as our results on side-band cooling[6] should be applicable to the bonded cavity due to the near identical cavity characteristics. For this reason, we concluded that the successful completion of WP 4.2 also fulfilled the test-readiness for the bonded cavity.

In order to complete work package WP 4.3, we implemented a novel particle loading mechanism so as not to contaminate the bonded cavity mirrors, and we designed and implemented a new vacuum chamber to integrate this loading mechanism with the cavity setup. As described in WP

3.3, due to an error in the design, the cavity holder did not fit the bonded cavity. For this reason, the corresponding tests could not be completed within the reporting period.

CONCLUSIONS

We successfully performed two detailed thermal studies that clearly showed that the thermal design of MAQRO should allow fulfilling the technical requirements of MAQRO. In fact, the results of our thermal studies went well beyond what we originally suggested for MAQROsteps. This work led to a publication in 2014 and another paper is currently under consideration for Applied Thermal Engineering.

With respect to feedback cooling and sideband cooling, which we now refer to as 3D cooling, we achieve significant progress. On the one hand, we devised a promising new technique for realizing 3D cooling in a cavity by using four optical modes – two TEM_{00} modes as well as a TEM_{01} mode and a TEM_{10} mode. The theoretical details of this new method will soon be published. Using this method should allow to achieve cooling rates higher than the damping rates of the surrounding gas at 1mbar. Because trapping particles at 1mbar is readily achieved, using this cooling mechanism should allow going to lower pressures. Moreover, we identified the main problem in achieving stable trapping at low pressures and achieved significant progress in mitigating this problem by trapping cleaner particles containing less contaminants.

In addition, we realized a novel technique for transporting particles and loading them into the cavity mode at ultra-high vacuum. This method uses transport along a hollow-core photonic-crystal fiber in combination with a grin-lens optical trap. This miniature trap can then be used to position a trapped particle in the cavity mode. Using this method will allow to load particles into our bonded cavity without the danger of contaminating the mirror surfaces with nanoparticles or with the solution carrying the particles. This would have been a serious issue using our old particle loading techniques.

In conclusion, we achieved significant technological progress on the road towards a possible future implementation of the MAQRO mission proposal.

Bibliography

1. Hechenblaikner, G. *et al.* How cold can you get in space? Quantum physics at cryogenic temperatures in space. *New J. Phys.* **16,** 013058 (2014).
2. Ball, P. Space: How cold does it get when we leave Earth? *BBC Futur.* (2013). at <http://www.bbc.com/future/story/20130920-how-cold-is-space-really>

3. Loose, M., Beletic, J., Garnett, J. & Muradian, N. Space qualification and performance results of the SIDECAR ASIC. in *SPIE Astron. Telesc. + Instrum.* (eds. Mather, J. C., MacEwen, H. A. & de Graauw, M. W. M.) 62652J–62652J–11 (International Society for Optics and Photonics, 2006). doi:10.1117/12.672705
4. ESATAN-TMS thermal engineering manual. *ITP Engines UK Ltd* (2010). at <www.esatan-tms.com>
5. Pilan Zanoni, A. *et al.* Performance of a radiatively cooled system for quantum optomechanical experiments in space. 13 (2015). at <http://arxiv.org/abs/1508.01032>
6. Kiesel, N. *et al.* Cavity cooling of an optically levitated submicron particle. *Proc. Natl. Acad. Sci. U. S. A.* **110,** 14180–5 (2013).
7. Gieseler, J., Novotny, L. & Quidant, R. Thermal nonlinearities in a nanomechanical oscillator. *Nat Phys* **9,** 12 (2013).
8. Millen, J., Deesuwan, T., Barker, P. & Anders, J. Nanoscale temperature measurements using non-equilibrium Brownian dynamics of a levitated nanosphere. *Nat. Nanotechnol.* **9,** 425–9 (2014).
9. Gieseler, J., Deutsch, B., Quidant, R. & Novotny, L. Subkelvin Parametric Feedback Cooling of a Laser-Trapped Nanoparticle. *Phys. Rev. Lett.* **109,** 103603 (2012).
10. Millen, J., Fonseca, P. Z. G., Mavrogordatos, T., Monteiro, T. S. & Barker, P. F. Cavity Cooling a Single Charged Levitated Nanosphere. *Phys. Rev. Lett.* **114,** 123602 (2015).
11. Yin, Z., Li, T. & Feng, M. Three-dimensional cooling and detection of a nanosphere with a single cavity. *Phys. Rev. A* **83,** 013816 (2011).
12. Kaltenbaek, R. *et al. Macroscopic quantum resonators (MAQRO): 2015 Update*. (2015). at <http://arxiv.org/abs/1503.02640>
13. Pound, R. V. Electronic Frequency Stabilization of Microwave Oscillators. *Rev. Sci. Instrum.* **17,** 490 (1946).
14. Drever, R. W. P. *et al.* Laser phase and frequency stabilization using an optical resonator. *Appl. Phys. B Photophysics Laser Chem.* **31,** 97–105 (1983).
15. Argence, B. *et al.* Prototype of an ultra-stable optical cavity for space applications. *Opt. Express* **20,** 25409–20 (2012).
16. Möhle, K., Kovalchuk, E. V., Döringshoff, K., Nagel, M. & Peters, A. Highly stable piezoelectrically tunable optical cavities. *Appl. Phys. B* **111,** 223–231 (2013).
17. Elliffe, E. J. *et al.* Hydroxide-catalysis bonding for stable optical systems for space. *Class. Quantum Gravity* **22,** S257–S267 (2005).
18. Ressel, S. *et al.* Ultrastable assembly and integration technology for ground- and space-based optical systems. *Appl. Opt.* **49,** 4296 (2010).
19. Drever, R. W. P. *et al.* Laser phase and frequency stabilization using an optical resonator. *Appl. Phys. B* **31,** 97–105 (1983).

2.3 Änderungen im weiteren Projektverlauf

Es kam zu geringfügigen Anpassung bei den Laufzeiten von WP 3.2 und WP 3.3, allerdings wurden die Arbeitspakete dennoch rechtzeitig innerhalb des Projektverlaufes fertig gestellt.
Aufgrund eines Designfehlers bei einem Cavityhalter für die gebondete Cavity konnte die gebondete Cavity nicht mehr rechtzeitig vor Projektende in die neue Vakuumkammer eingebaut werden, um sie im Zusammenhang mit dem optomechanischen Setup zu testen. Da die Cavity allerdings vollständig charakterisiert wurde und praktisch in allen Belangen ident zur Standardcavity ist, die im optomechanischen Setup verwendet wird, werden hier keine Abweichungen erwartet. Fall es Abweichungen geben sollte, würden wir erwarten, dass diese sogar eher positiv ausfallen, da die gebondete Cavity augenscheinlich wesentlich stabiler gegenpber thermalen Fluktuationen ist. Dies könnte vor allem auch im Zusammenhang mit dem neuen Lademechanismus – der grin-lens Falle – positiv sein, da das gestreute Licht der grin-lens Falle, die Cavity leicht aufheizt. Die gebondete Cavity sollte diesem Effekt gegenüber stabiler sein. Bemühungen sind derzeit im Gange, damit die gebondete Cavity sobald wie möglich in das optomechanische Experiment integriert werden kann.

3. Projektteam und Kooperation

- Gibt es wesentliche Veränderungen im Projektteam je Partner gesehen (interne Schlüsselmitarbeiter und Drittleister)?
- Gehen Sie auf Änderungen in der Arbeitsaufteilung ein. Gibt es Auswirkungen auf die Kosten- / Finanzierungsstruktur und die Zielsetzung?

Im Berichtzeitraum gab es weder wesentliche Veränderungen im Projektteam noch Änderungen bei der Arbeitsaufteilung. Beim Drittleister Airbus D & S (früher EADS Astrium), wurde Gerald Hechenblaikner im August 2014 durch Michael Chwalla ersetzt, welcher nun seine Aufgaben in Bezug auf MAQROsteps übernimmt. Für die Durchführung von MAQROsteps ergeben sich dadurch jedoch keine wesentlichen Änderungen.

4. Erläuterungen zu Kosten & Finanzierung

- Die Abrechnung ist als eigene Datei im Excel-Format hochzuladen. Die Verwendung der im eCall zur Verfügung gestellten Vorlage ist verpflichtend. Beachten Sie den Kostenleitfaden: www.ffg.at/kostenleitfaden bzw. Ausschreibungsdokumente
- Abweichungen vom Kostenplan sind an dieser Stelle zu beschreiben und zu begründen.
- Ist mit Änderungen am Kostenplan bis zum Projektende zu rechnen? Wenn ja, erläutern Sie diese. (Achtung: Größere Änderungen sind genehmigungspflichtig)

Das geplante Budget enthielt Reisekosten für zwei Reisen nach Friedrichshafen (Deutschland) im Zuge der Kollaboration mit dem Drittleister Airbus D & S. Eine der Reisen war für zwei Personen kalkuliert, allerdings konnte am tatsächlichen Termin seitens der Universität Wien nur der Projektleiter teilnehmen. Dadurch entstand eine leichte Abweichung vom geplanten Budget. Im Allgemeinen war für das Projekt etwas zu wenig Reisebudget veranschlagt worden. Abgesehen von den erwähnten Reisen des Projektleiters, wurden noch einige andere Reisen, die im Zusammenhang mit dem Projekt standen, getätigt, und der Projektleiter hat den FFG gebeten, für diese Reisekosten Mittel im Umfang von bis zu 5000€ aus den Materialkosten in Reisekosten umzuwidmen.

Bei den Materialkosten gibt es Abweichungen, da die ursprünglich veranschlagten Kosten für zwei electro-optic modulators (EOMs) von anderen Projekten bezahlt wurden und wir diese EOMs für MAQROsteps unentgeltlich für die Experimente im Rahmen von MAQROsteps verwenden konnten. Die freigewordenen Materialkosten werden stattdessen für Material verwendet, welches für die Projektdurchführung von MAQROsteps notwendig ist. Insbesondere wird es dabei um entstehende Kosten für die Anfertigung der MAQRO cavity gehen, wie am Ende von Abschnitt 3 beschrieben wurde. Dieses Material wurde im ursprünglichen Budget nicht angeführt, weil die Anforderungen an die Genauigkeit bei der Zusammensetzung der MAQRO Cavity höher als erwartet sind. Um diese Genauigkeit zu erreichen werden im nächsten Berichtzeitraum Kosten für optomechanische Komponenten anfallen. Dies wird im Zuge des Endberichtes eingehend erläutert werden.

5. Projektspezifische Sonderbedingungen und Auflagen

- Gehen Sie auf projektspezifische Sonderbedingungen und Auflagen (laut §6 des Förderungsvertrags) ein, sofern diese im Förderungs- bzw. Werkvertrag vereinbart wurden

Es wurden keine Sonderbedingungen vereinbart.

6. Meldungspflichtige Ereignisse

Gibt es besondere Ereignisse rund um das geförderte Projekt, die der FFG mitzuteilen, z.B.

- Änderungen der rechtlichen und wirtschaftlichen Einflussmöglichkeiten beim Förderungsnehmer
- Insolvenzverfahren
- Ereignissen, die die Durchführung der geförderten Leistung verzögern oder unmöglich machen
- Weitere Förderungen für dieses Projekt

Im Berichtzeitraum gab es keine meldungspflichtigen Ereignisse.